404

March 1981

DOT HS 806 324

Final Technical Report

Volume 1 Of 2

US Department of Transportation
National Highway Traffic Safety Administration

Anatomical Cross-Sectional Geometry and Mass Distribution for Children

H.K. Huang
Dept. of Radiological Sciences
UCLA
Los Angeles, CA 90024

Contract: DTNH-7-01661

404

Technical Report Documentation Page

1 Report No	2 Government Accession No	3 Recipient's Catalog No
DOT-HS-806 324		

4 Title and Subtitle
Anatomical Cross-Sectional Geometry and Mass Distribution for Children

5 Report Date
March 31, 1981

6 Performing Organization Code

8 Performing Organization Report No

7 Author(s)
H.K. Huang

Department of Radiological Sciences
UCLA, Los Angeles, CA 90024

9 Performing Organization Name and Address

Dept. of Physio. & Biophysics
Georgetown Univ. Medical Ctr.
3900 Reservoir Road., N.W.
Washington, DC 20007

Biomedical Engineering
College of Engineering
University of Iowa
Iowa City, IA 52242

10 Work Unit No TRAIS

11 Contract or Grant No
DOT-HS-7-01661

13 Type of Report and Period Covered
Final Report
9/23/77 - 3/31/81

12 Sponsoring Agency Name and Address

Department of Transportation
National Highway Traffic Safety Administration

14 Sponsoring Agency Code

15 Supplementary Notes
Volume 1 of two volumes

16 Abstract

Conventional methods for evaluating human body geometry are multi-plane x-ray images, segmented cadaveric trunks and biostereometrics. These approaches are crude estimated methods and do not reveal detailed tissue structures and mass density distribution of the body. With the recent developed x-ray computerized tomography (CT), it is possible to use this method to extract detailed body structures and their mass density distributions.

The purpose of this study was to generate anatomical cross-sectional geometry and mass density distribution of children using the CT method. Five cadaveric specimens, with age ranging from newborn to seven, were studied. Cross-sectional CT scans of these specimens were obtained at one centimeter interval from the head to the ankle joints. From these cross-sectional CT images, the outlines of each cross section and of selected anatomical components within each section were obtained by standard picture processing techniques. The mass and inertia tensors for each cross section were estimated based on a conversion from x-ray absorption coefficients of tissues appearing on a CT scan to their mass densities.

In order to store and retrieve this mass of information, a data base structure had been designed. Also presented was a discretization procedure and the generation of an internal mesh which could be used for subsequent finite element analysis.

Some immediate applications of this data are inputs to finite elements and lumped parameter biodynamics models, computer simulation of vehicle crash victims and designing crash dummies. Moreover, the CT approach provides an excellent potential for in vivo injury recovery study. Vol. I of this report contains the methodology and Vol.II contains derived anatomical geometry and mass distribution.

17 Key Words	18 Distribution Statement
X-ray Computerized Tomography, Cross-Sectional Anatomy of Children, Cross-Sectional Mass and inertia tensor, biomechanic data base, quantitative anatomy	This document is available to the public through the National Technical Information Service, Springfield, Virginia 22151

19 Security Classif (of this report)	20 Security Classif (of this page)	21 No of Pages	22 Price
Unclassified	Unclassified	82	

Form DOT F 1700.7 (8-72) Reproduction of completed page authorized

Volume I of this report contains the methodology, and CT scans of the five specimens. Volume II contains derived anatomical geometry and mass distribution data from cross-sectional scans.

ACKNOWLEDGEMENT

The idea of using X-ray CT to obtain cross-sectional anatomy, mass, and inertia property of human specimen was originated in an informal meeting between Dr. Lee Ovenshire of NHTSA, DOT, Mr. Arthur E. Hirsch (formerly with NHTSA, DOT) and the author in 1975. Dr. Ovenshire and Mr. Hirsch later convinced the management of NHTSA to support this research. Dr. Faustino R. Suarez, Department of Anatomy, Georgetown University Medical Center has made invaluable contribution in this project. The finite element analysis is mostly Drs. Theodore G. Toridis and Khalil Khozeimeh's (George Washington University) work. The author would also like to thank Peter Weiss, Mathew Cerroni and Becky Wilson for their contributions.

ANATOMICAL CROSS-SECTIONAL GEOMETRY
AND MASS DISTRIBUTION FOR
CHILDREN

DOT-HS-7-01661
Vol. 1

Page

ACKNOWLEDGEMENT

TABLE OF CONTENTS

LIST OF FIGURES

LIST OF TABLES

SECTION A

INTRODUCTION

1. Objectives

This research was to determine the cross-sectional geometry and mass density distribution of children cadaveric specimens using the x-ray computerized tomographical (CT) method. In particular, the following were specific objectives:

1) Use x-ray CT to scan cross sections of five child specimens. The distance between each consecutive section is approximately 1 centimeter.
2) Digitize external boundary and selected anatomical structures from each cross section.
3) Estimate mass density and inertia tensors for each cross section.
4) Develop a data base structure to store this information.
5) Generate finite elements mesh from cross-sectional geometry.

2. Background

Conventional methods for evaluating cross-sectional human geometry are multi-plane x-ray images and segmented cadaveric trucks (1,2) and biostereometrics (3). Because these approaches are crude estimating methods, they do not reveal detailed tissue structures and their mass density distribution within a cross section. With the recent development of x-ray computerized tomography (CT)(4,5), it is now possible to use this method to obtain outlines of body structures and their mass density distribution. The CT method is an excellent approach for several reasons. First, there is practically no geometrical distortion between the body section and its CT image since the CT scanning procedure is nondestructive. Second, CT images

are already in a digital format, and therefore there is no need to perform the analog to digital conversion procedure. Third, the CT image of a cross section has a spatial resolution of from 1.0 x 1.0 mm^2 to 1.5 x 1.5 mm^2, and the thickness of each section is between 7 to 13 mm. This high spatial resolution of the data is more than adequate for any types of current biomechanics research application. Fourth, methods have already been developed which will allow the estimation of mass density distribution of a cross section directly from its CT scans (6) and the direct computation of the inertia tensor of the cross section. Finally, since the x-ray dosage delivered to the scanning object is very nominal, the CT method is a good potential method for determining the in vivo cross-sectional geometry of humans and animals.

3. Specific Aims

The specific aims of this study were:

3.1 Geometrical Description of Cross Sections

X-ray computerized tomography was used to scan cross sections of child cadavers. The distance between each consecutive cross section was approximately 1 cm, and the specimen was placed in the supine anatomical position during the scanning. Five child cadavers of various ages were scanned, and body lengths were 27, 43, 89, 104 and 132 cm.

3.2 Digitize Selected Anatomical Components

Boundary detection computer programs with interactive features were developed to extract external contours, boundaries of skeletal structures and vital organs from CT scans.

3.3 Estimate Inertia Tensor and Mass

The mass, geometrical center, center of gravity, and inertia tensor for each cross-sectional scan were estimated. The first step in obtaining

these values was to convert CT numbers into mass densities for all points in the CT scan. These parameters were then estimated by using standard formulas for discrete masses in mechanics.

3.4 Develop a Data Base Structure to Store This Information

A data base structure was developed to systematically store cross-sectional scans, digitized anatomical components, masses and inertia tensor. Algorithm were also planned for optional information retrieval.

3.5 Generate Finite Elements Mesh from Cross-Sectional Geometry

Algorithms and computer programs were developed for discretization procedure and the generation of an internal mesh for anatomical components. The input data for this mesh generator were boundary coordinates of anatomical structures extracted from CT scans.

SECTION B

COMPUTERIZED TOMOGRAPHICAL SCANNING

1. The FS0200 Scanner

The FS0200 CT scanner, a second generation scanner manufactured by Pfizer Medical Systems, Incorporated was used for the CT scan, it takes 20 seconds per scan. The components of the scanner are shown in Figure B-1 (7). After the completion of each scan the picture was stored in a magnetic tape for

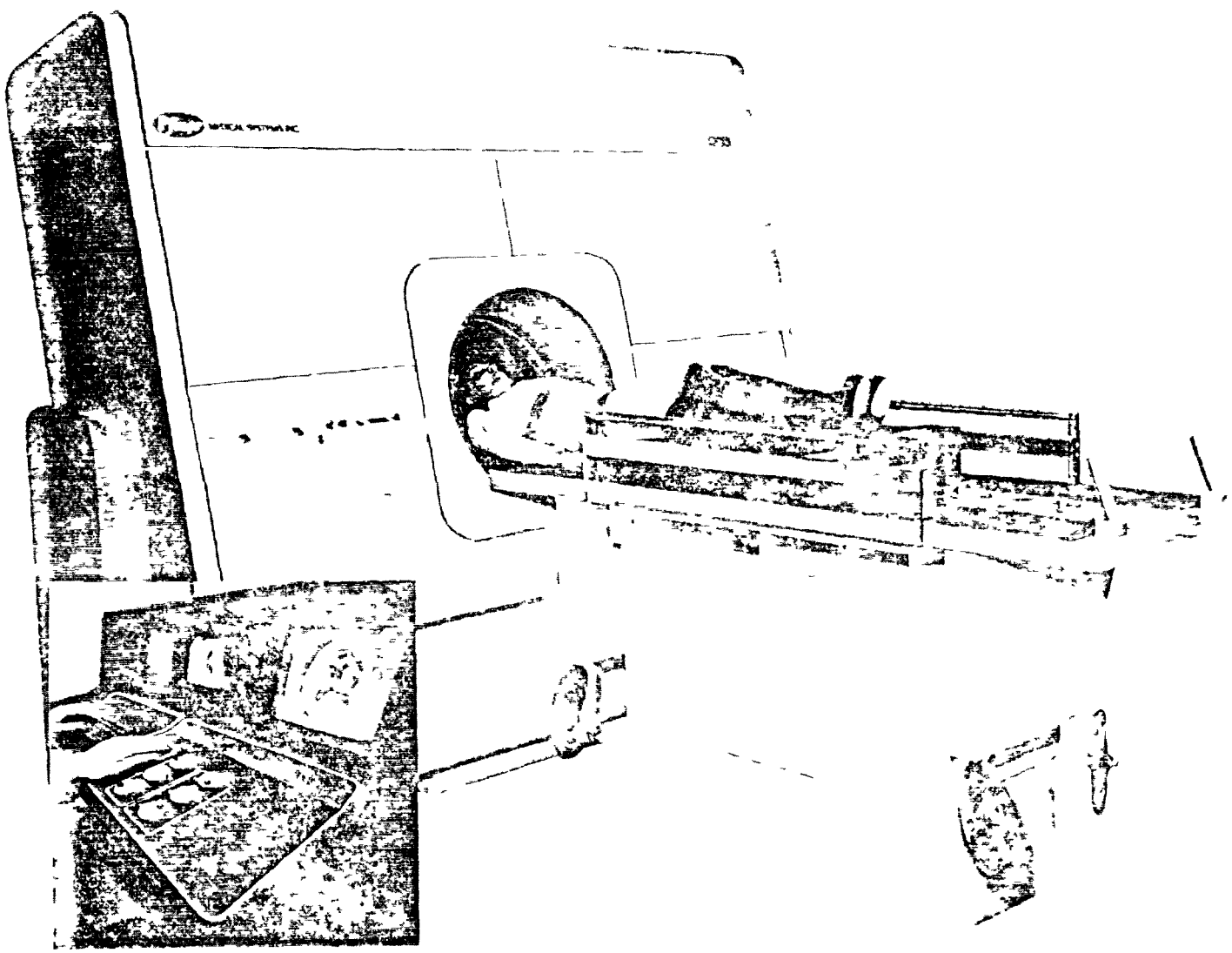

Figure B-1 The FS0200 CT Scanner

2. Picture Format of the FS0200 ACTA Scanner

2.1 Picture Formats

The computer system of the FS0200 Scanner consists of a PDP11/34 computer with 64K 16-bit words, and a 800/1600 BPI tape drive. The most commonly used picture formats of this scanner are the H256 head scan and the B320 body scan (8). The H256 is for high-resolution head scans and its data format is a 256 x 256 picture. Each pixel (picture element) represents a 1 mm x 1 mm tissue area with a thickness of 10 mm, (See Figure B-2.a). The B320 is for body scans and its data format is a 320 x 320 picture. Each pixel in B320 represents a 1.5 mm x 1.5 mm tissue area with a thickness of 10 mm(See Figure B-2.b).

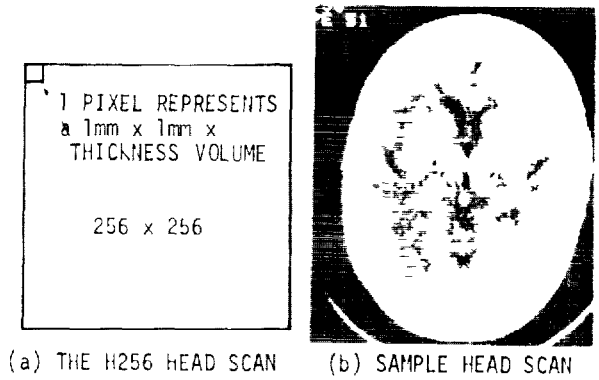

(a) THE H256 HEAD SCAN (b) SAMPLE HEAD SCAN

Figure B-2.a: Picture format of the FS0200 Scanner H256 head scan. Each pixel represents a 1.0mm x 1.0mm tissue area with a thickness of 10mm.

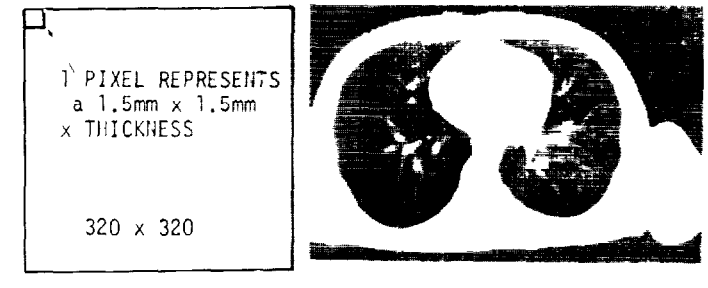

(a) THE B320 BODY SCAN (b) SAMPLE BODY SCAN

Figure B-2.b: Picture format of the FS0200 Scanner B320 body scan. Each pixel represents a 1.5mm x 1.5mm tissue area with a thickness of 10 mm.

2.2 Data Formats

The data formats of the H256 head scan and the B320 body scan are shown in Figure B-3.

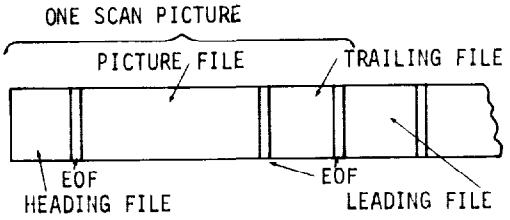

Figure B-3 Tape format of a FS0200 Scanner

The picture file contains the scan picture and can have one of three forms. The first two forms, written on tape, use the PDP MT handler for the magnetic tape unit*, and can also be read by the conventional PDP Peripherial Interchange Program (PIP)*. The third form uses a special FS0200 program and cannot be read by the PIP.

The first form is a direct columnwise copying. Each data block contains one column of the picture as seen on the TV screen+, and may include the heading and other annotations. As a result, this data format requires the most space from the tape for storing.

The second form, which is the most commonly used and desired form for off-line processing of the scan, has the structure of the picture file shown in Figure B-4. The picture is divided into picture descriptors and picture information. This data format is compact and easily accessible, since it can be read by the standard PIP system. With this data format, a 240 foot tape can store approximately 80 to 90 B320 body scans.

---

*Standard PDP Format

+After each scan the picture and the corresponding picture heading is shown on TV screens.

The last form is written on tape by using the PDP/MX handler for the magnetic tape unit and cannot be read by the PIP system. Its picture file has the same form shown in Figure B-4 except that the block size is larger. This format can only be read by the FS0200 computer programs and it is not accessible by standard PDP system programs. Providing the most extensive packing this format can store more pictures on a tape, therefore, it is the standard format used in a clinical environment. However, for off-line processing this is not a very desirable format, since it depends totally on the FS0200 system for retrieval. All CT scans of specimens used in this project were stored using the second format.

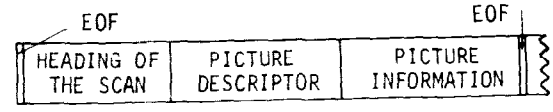

Figure B-4 Structure of a FS0200 Picture File

SECTION C

SPECIMENS AND SCANNING PROCEDURES

1. Techniques for Acquiring and Preparing Scanning Specimens

A total of eight specimens were scanned during the study period. From these specimens, five were selected for the cross-sectional geometry and mass distribution study. The physical condition of these five specimens is depicted in Table C-1.

Table C-1 -- Five Specimens for the Cross-Sectional Geometry and Mass Distribution Study

SPECIMEN NUMBER	AGE	SEX	BODY LENGTH (CM)	BODY WEIGHT AND LENGTH OF NORMAL CHILD (9)		
				Kg	Cm	
6	New born	M	27	3.4 ± .5	50 ± 3	
1	2 months	M	57	5.7 ± 1	60 ± 3	
5	3 years	F	89	14 ± 2	95 ± 5	
4	5 or 6 years	M	110	18.4 ± 3 21.9 ± 3.5	108 ± 6 117 ± 7	(5 year) (6 year)
2	7 years	M	156	24.5 ± 4.5	124 ± 6	

1.1 Physical Description of Each Specimen

Every effort has been made to obtain pertinent information from each specimen. However, the physical description of each specimen is limited due to the scarcity of child cadavers and the duration of availability of each specimen. The physical condition of the five selected specimens are described in this section.

Specimen 6

Donated to Georgetown University Hospital

Cause of Death: still-born

Scanning Condition : 40°F, (received within seventy-two hours of death)

Length: Total body length--27 cm

Specimen 1

Donated to the Department of Anatomy, Georgetown University Medical School

Cause of Death: Hydrocephalus

Scanning Condition: Embalmed

Length: Total body length -- 57 cm
Head -- 16 cm
Trunk -- 21 cm
Thigh -- 10 cm
Leg -- 10 cm

Specimen 5

Borrowed from Department of Anatomy, Georgetown University Medical School

Cause of Death: Leukemia

Scanning Condition: Embalmed

Length: Total body length -- 89 cm
Hip joint - Knee joint -- 25 cm
Knee - Ankle joint -- 23 cm
Shoulder - Elbow joint -- 15 cm
Elbow -- Wrist joint -- 15 cm

Circumference: Head -- 54 cm
Chest -- 55 cm

Specimen 4

Borrowed from the Department of Anatomy, Medical College of Virginia at Richmond

Cause of Death: Mentally retarded

Scanning Condition: Embalmed

Length: Total body length -- 110 cm

Specimen 2

Donated to the Department of Anatomy, Georgetown University Medical School

Cause of Death: Leukemia

Scanning Condition: 40°F, (received within seventy-two hours of death)

Length: Total body length -- 156 cm
Leg Length: anterior-superior iliac spine-heel -- 67 cm
anterior-supreior iliac spine-knee -- 35 cm
knee-heel -- 32 cm
Arm Length: acromion-tip of finger -- 51 cm

Circumference: head -- 53 cm
chest at nippel line -- 65 cm
iliac spine -- 61 cm
upper 1/3 thigh -- 34 cm
mid 1/3 thigh -- 35 cm
lower 1/3 thigh -- 29 cm
arm -- 22 cm

Width: shoulder to shoulder -- 27 cm

2. Scanning Procedure

The scanning procedure of each specimen was as follows:

(1) A water phantom was scanned for calibration purposes prior to the scanning of a specimen.

(2) Each specimen was placed in a supine position, and the head was scanned first.

(3) In order to determine the desired scanning level, some prominent body landmarks were placed on the skin of the specimen with a standard felt-tip pen.

(4) The body was moved on the motorized scanning table, based on these landmarks, to the desired scanning level.

(5) The specimen was scanned at one centimeter increments from the cranium to the ankle joints.

(6) This scanning procedure was continued until a second body landmark was encountered. If the next scanning level was within five millimeters of

the previous body landmark no adjustments were made to the motorized table, thus, the scanning procedure was continued. If the next scanning level was more than five millimeters from this landmark an additional scan was preformed at the landmark.

(7) This scanning procedure was continued until the ankle joints were reached.

2.1 Coordinate System for the Scan Pictures

Figure C-1 shows the coordinate system used for the scan pictures. The x-axis, y-axis and z-axis represent the left-right, anterior-posterior, and superior-inferior position of the scanning specimen. If the plane perpendicular to the cranial end is used as the z = 0 plane, the z-coordinates of scanning cross sections would be increasing towards the inferior end of the specimen. The right-anterior corner would have the coordinates (1,1) and the left-posterior corner would have the coordinates (160,160), (256,256), or (320,320) depending on the size of the specimen.

2.2 Scanning Results

In a scan picture DEL X and DEL Y represent the spatial resolution on the x-y plane. Therefore, when DEL X = DEL Y = 1.0 mm, each picture point in the x-y plane represents a tissue ares of 1 mm^2. The distance between two cross-sectional scans is represented by DELZ. Table C-2 shows the total number of scans in each specimen.

2.3 Additional Scanning Results

2.3.1 Prone and Sitting Positions

In addition to the supine position, specimen No. 2 was also scanned in the prone (40°F) and the sitting position (frozen). In the case of the prone position only the trunk of the specimen was scanned, whereas in the

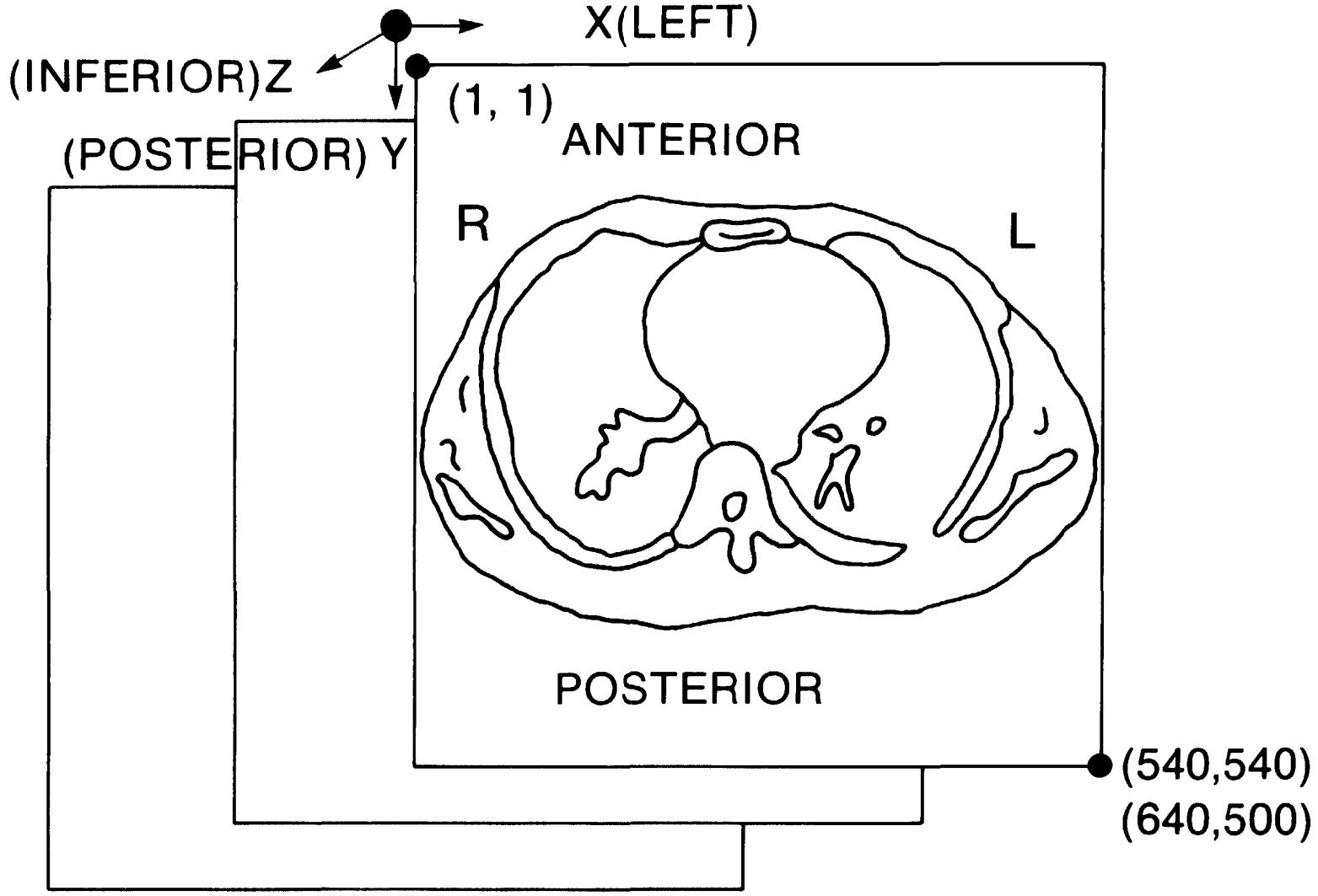

COORDINATE SYSTEM USED FOR SCAN PICTURES

The X-axis, Y-axis, and Z-axis represent the left-right, anterior-posterior, and superior-inferior (cephalad-caudal) of the specimen.

Figure C-1: Coordinate System Used For Scan Pictures

Table C-2

Total Number of Scans in the Five Specimens

Specimen Number	Age/ Sex	Body Length cm	Number of Scans					
			Head & Neck	Chest	Abdomen	Pelvis	Lower Extremity	Total
6	N/M	27	6	6	2	3	10	27
1	2M/M	57	17	7	8	5	5	42
5	3Y/F	89	20	10	14	16	39	99
4	5-6Y/M	110	28	10	15	17	59	129
2	7Y/M	156	29	18	19	20	72	158

sitting position the specimen was scanned from the cranium to the hip joints. The following procedure was used during th scanning of the body in the sitting position. The specimen was first frozen overnight in a sitting position as shown in Figure C-2.a. The frozen cadaver was then scanned the next day in a supine position as shown in Figure C-2.b. Since the body was still frozen, the relative positions of anatomical structures should resemble the state of a sitting position. Scans were taken from the head to the hip joints at one centimeter intervals. Due to the placement of the cadaver, the long axis of the thighs below the hip joints were almost parallel to the direction of the x-ray beams.* As a result of this scanning position, frontal plans of the thighs of the body was obtained. Images of these frontal sections will allow the study of impact response in a sitting position such as in an automobile environment.

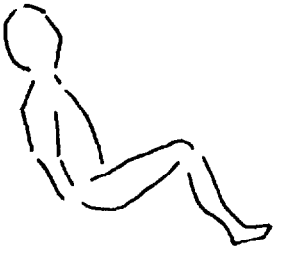

Figure C-2.a The body was frozen in a sitting position.

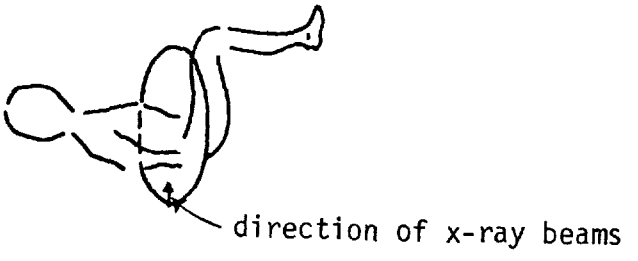

Figure C-2.b. The frozen body was scanned in a supine position.

*For a conventional scan the axis of the body is perpendicular to the X-ray beams.

2.3.2 Anatomical Differences Observed From Three Scanning Positions

Based on the three different scanning positions -- supine position (40°F), prone position (40°F), and sitting position (frozen) -- of specimen number 2 the following observations could be made:

I. Anatomical Differences Observed From Three Scanning Positions

a. Head and Neck Region

1. The anatomy in the slices of the head and the neck in the supine and sitting positions were slightly different due to the difference in scanning angles from positioning.
2. In the sitting frozen position, the ventricles of the brain were better visualized than that in the unfrozen specimen. The sulci are also better delineated in the frozen sitting position.
3. In the sitting frozen position the walls of the eyeball seemed to be thicker than that of the unfrozen specimen.
4. In the supine position the esophagus was collapsed while in the sitting frozen state the lumen was open.

b. Thorax

1. During the prone position scans, the arms were raised above the head, while in the supine and sitting position scans the arms were at the sides. The difference in the arms position would effect the relative positions of the bones and organs in the thorax.
2. Esophagus in the frozen state the lumen were open while in the supine and prone positions they were closed or collapsed.
3. In the sitting position, the contour of the heart was found on the midline while in the supine and prone positions, it was

deviated to the left. The heart was deviated more to the left in the prone position than in the supine position.

4. The primary bronchi in the sitting position were deviated more posteriorly than in the supine position while in the prone position they were less deviated posteriorly than in the supine.

5. Diaphragm in the sitting position seems to be lower than in the supine and prone position. The right side and left side of the diaphragm in the sitting position had a difference of one slice while in the prone and supine it had two slices in difference.

C. Abdominal and Pelvic Region

1. In the sitting position, the esophagus showed the lumen opened wider than in the prone and supine position.

2. Kidney on the right side seemed to be in a higher position or level in the prone position than in the supine position.

3. In the sitting position there was a space between the spleen and the abdominal wall while in the prone and supine position there was no such space.

4. Slices were missing in the supine position between the costal arch and the iliac crest.

5. In the sitting and supine position intestines were concentrated at the posterior area of the abdominal cavity while in the prone position they were positioned more anteriorly.

6. In the supine and sitting position the intestines in the pelvic region located posteriorly while in the prone position they located anteriorly and to the left side of the pelvis.

II. Anatomical Differences Between the Frozen and the Unfrozen State of a Specimen

a. The sulci and ventricles were better defined in the frozen state than in the unfrozen state.

b. Eyeball wall was thicker in the frozen state than in the unfrozen state.

c. The esophagus lumen opened wider from the neck down to the stomach in the frozen state than in the unfrozen state.

d. The intestine seemed to be grouped together in the frozen state and this was not the case in the unfrozen state.

SECTION D

DERIVATION OF CROSS-SECTIONAL GEOMETRY AND MASS DENSITY DISTRIBUTION FROM SCAN PICTURES

The computer software package for deriving the cross-sectional geometry and mass density distribution from scan pictures was developed by using the PDP 11/34 computer system of the FS0200 Scanner (refere to Section B). This software package was also integrated into the FS0200 Scanner's Computer Software System as a complete package. Since CT pictures were saved on magnetic tapes with the data format described earlier after scans, this software package used tapes as the input medium. Figure D.1 depicts the operational procedure.

1. Technique for Identifying Anatomical Components

1.1 Method of Derivation

a. Eliminate the Head Holder/Scanning Bed From the Scan

When a supporting device for the specimen, such as the head holder or the scanning bed, was in the scanning path, its image would also be included in the picture. The first step was then to eliminate this device from the picture so that it would not be included in the data processing. This was accomplished by an interactive method. The operator first read the scan picture from the magnetic tape onto a TV screen. The head holder was in the lower portion of the picture. A series of points between the cross section of the head and the head holder were manually inputted onto the TV screen by using a joystick.

The computer program drew lines to separate the cross sections

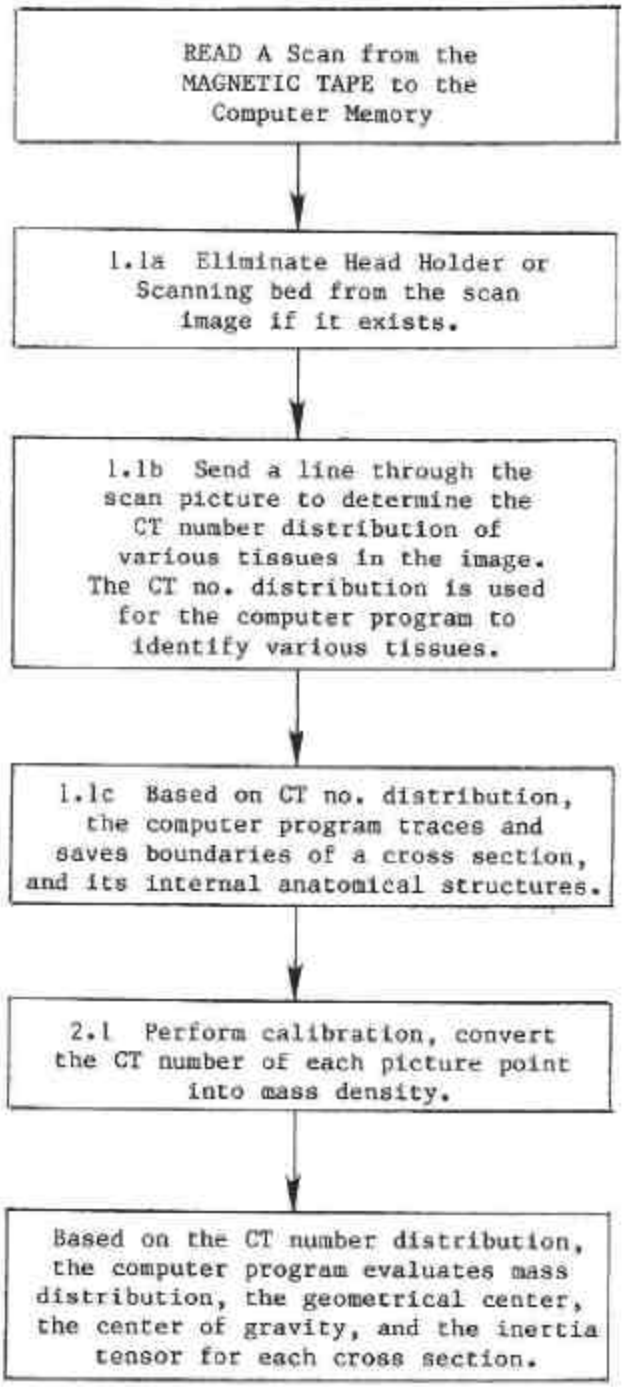

Figure D-1 Operational procedure in deriving Cross-sectional geometry and Mass Density Distribution from a Scan Picture.

from the head holder for these points. The header holder was then discarded from the image by the program. Only information pertinent to the cross section of the head was processed.

b. Evaluate the CT Number Distribution in the Cross-Sectional Image

The second step was to find the CT number distribution in the cross-sectional image. From this distribution the ranges of CT numbers of various issues in the cross section could be determined. These ranges were then used by the computer program to obtain outlines of the cross section, various internal organs, and bones.

In order to obtain the CT number distribution, a line was drawn on the scan picture passing through various anatomical structures of interest (Figure D-2.a). The CT number distribution of the scan picture along this line was recorded (Figure D-2.b). From the information in this distribution the computer program extracted boundaries of the cross section, various internal organs, and bones.

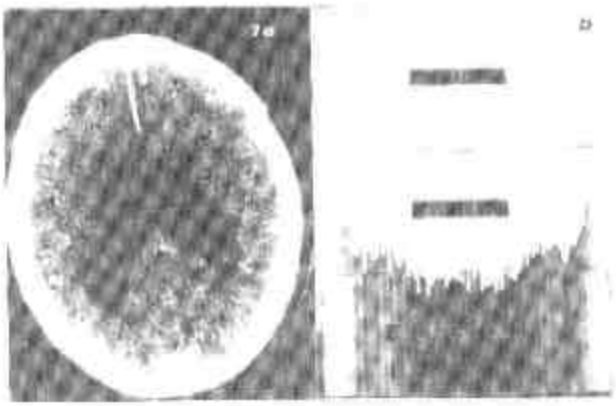

Figure D-2 Evaluate the CT Number Distribution in the Cross-Sectional Image a,b

Extracted Boundaries of Cross Section--Various Internal Organs and Bones

The first step in extracting the boundary of the cross section was to separate the arms from the body in the image (Figure D-3.a). This was accomplished by inputting four points exterior to each arm on the TV screen. From these four points, a quadrilateral enclosing the arm was drawn by the program. The computer program therefore divided a cross-sectional scan into three subimages, two arms, and the body (Figure D-3.b). Treating each of these images as an entity, the computer program extracted boundaries of the body and the two arms using the standard pattern recognition method (10,11,12). If an anatomical component of interest is also seen in the cross section, its boundary could also be traced by the computer program. In this case, the operator initiated a cursor on the TV screen and moved it near the antomical component of interest. Since the range of CT numbers of this anatomical component was already known (see Section D-1.1.b), the computer program could trace the boundary of the antomical component based on the range of its CT numbers (figure D-2.a). If other close-by anatomical components also had similar ranges of CT numbers, the computer program might be confused and failed to trace the proper boundary of the anatomical component. In this case, the operator could activate an interactive mode in the program. In the interactive mode, the operator used a track ball to outline the anatomical component of interest manually and the computer program would then save the coordinates of the boundary.

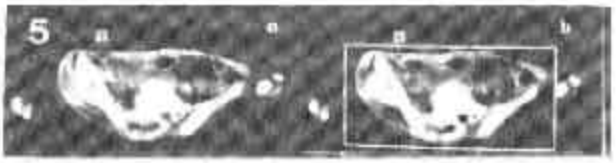

Figure D-3 Extract Boundaries of a Cross Section, Various Internal a,b Organs and Bones

1.2 An Example of Cross-Sectional Outlines

Figure D-3.c shows an example of cross-sectional scans of a lower leg below the knee joint and the corresponding boundaries of each cross section and its skeletal structures extracted by this procedure.

2. Technique for Computing The Mass, Center of Gravity, and Inertia Tensor of Anatomical Components

2.1 Technique for Determining Mass Density (6)

In order to obtain the center of gravity and the inertia tensor of each cross section from a CT scan, it was necessary to convert CT numbers in the scan to mass densities.

In this section the method for evaluating the mass density distribution of each cross section from CT number will be described. The numerical representations of an object in a CT scan is extrinsically a function of the effective x-ray energy during the scan, the picture reconstruction method, and the relative position of this material in the scan picture. Intrinsically, the numerical representations also depend on the constituents of the material under consideration, i.e., its atomic number, electron density and mass density.

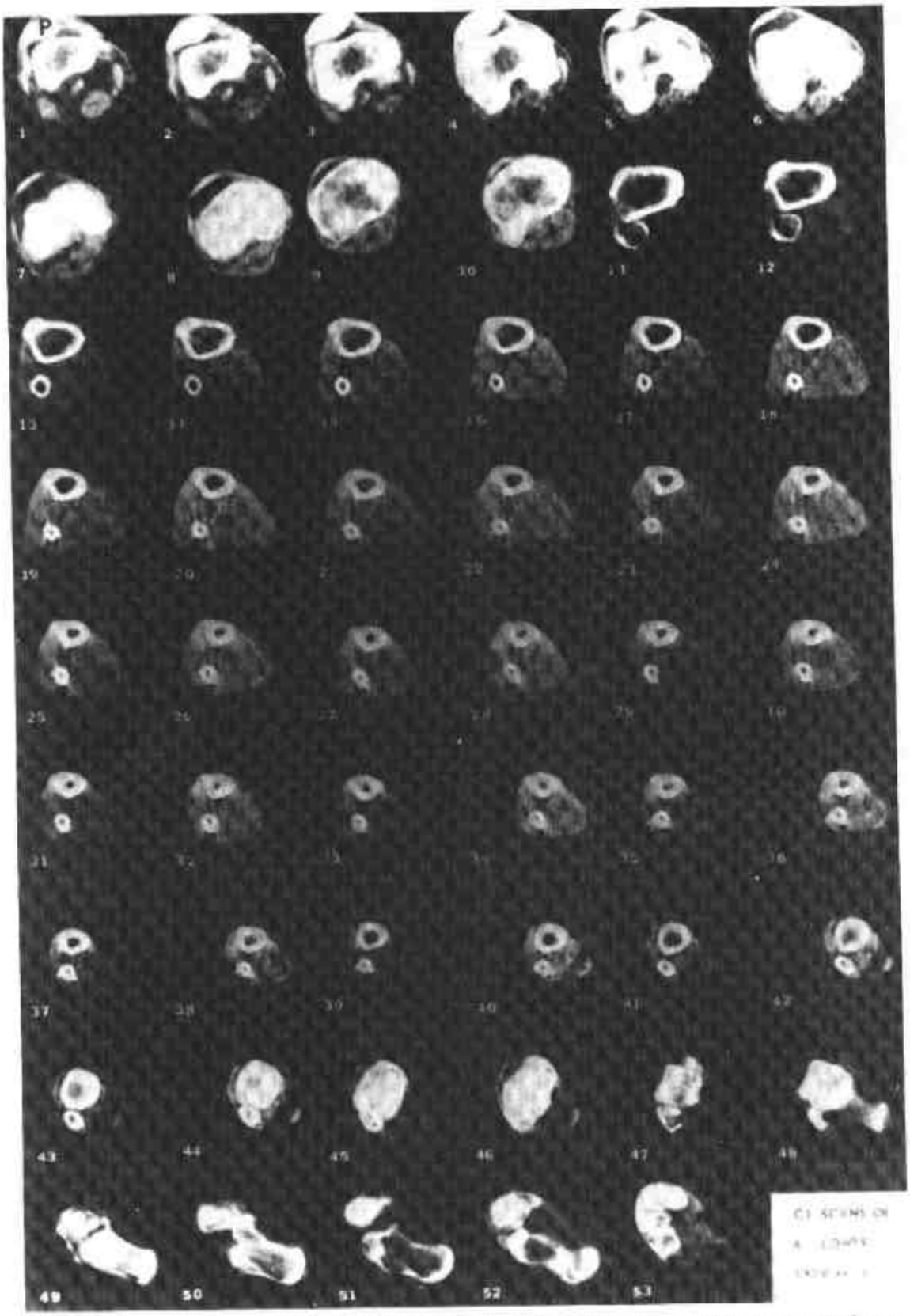

Figure D-3.c. Fifty-three scans of the lower extremity of a specimen, each scan is approximately 1 cm thick.

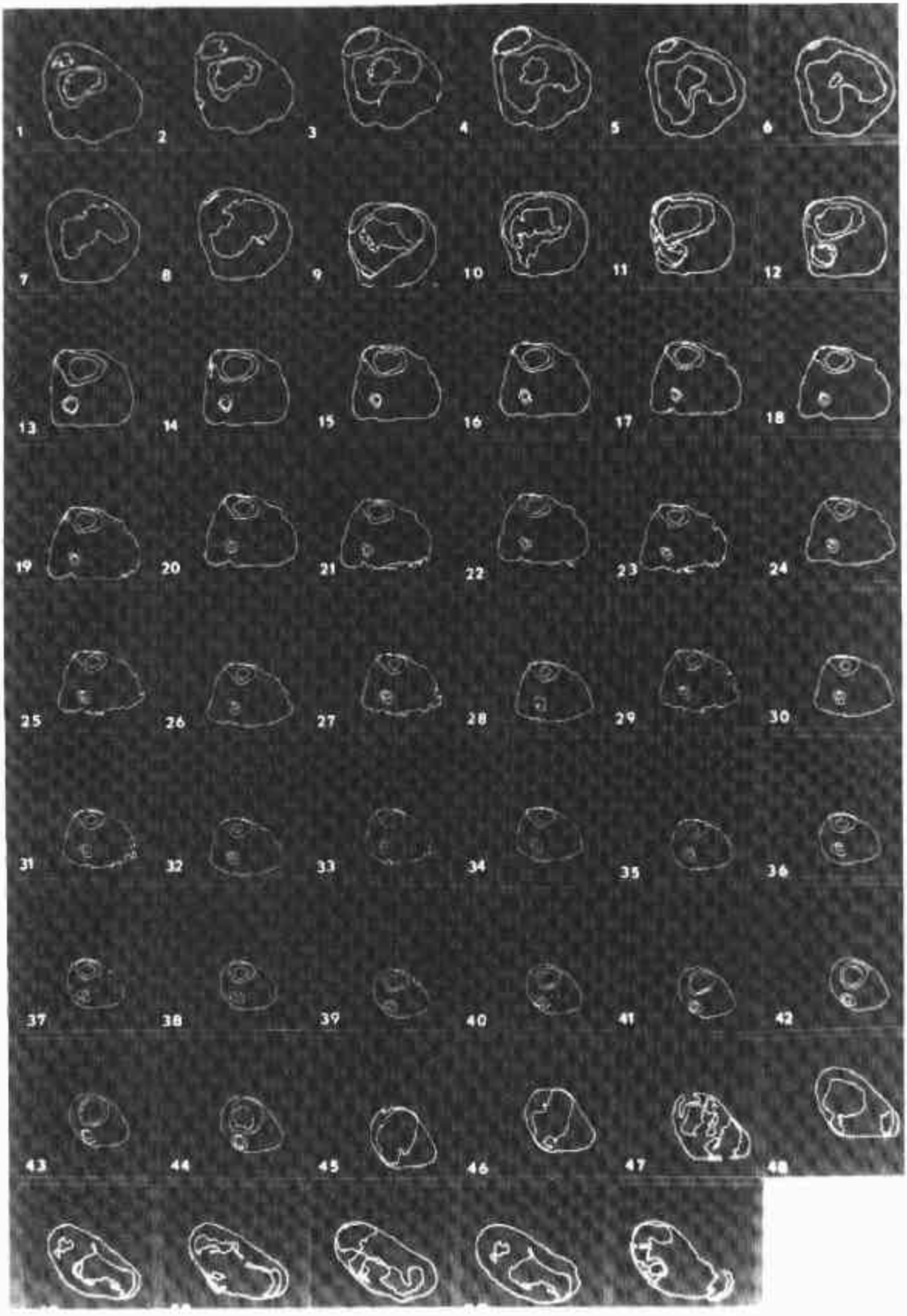

Figure D-3.c. Boundaries of each cross-sectional scan as well as the boundaries of skeletal components of each scan as shown in the left.

The present technique of estimating mass density of body constituents from a CT scan was based on an empirical method that the linear x-ray attenuation coefficient of a material is proportional to its CT number in a scan picture. This proportionality had been experimentally determined and the details were discussed in Reference (6).

Basically this procedure involved a conversion from the CT number of a tissue to its mass density pixel by pixel. This conversion can be represented by the following formula based on experimental results:

$$\rho_{tissue} = A\ (CT\ No.)_{tissue} + B$$

Where ρ_{tissue} : mass density of a tissue

$(CT\ no.)_{tissue}$: CT number of the same tissue

A and B are coefficients obtained from a calibration procedure.

During the calibration, A and B can be evaluated by:

$$A = (x_1 - x_o) / (y_1 - y_o)$$

$$B = ((x_1 - x_o) / (y_1 - y_o))\ y_o + x_o$$

Where x_o, x_1 are the mass densities of two known materials and

y_o, y_1 are the CT numbers of the two same materials obtained from a calibration CT scan.

Once A and B have been determined for a particular scan, the CT numbers in a picture can be converted to the corresponding mass densities on a point by point basis. This method of conversion is excellent for soft tissues; however, it is not ideal for compact bone due to the x-ray beam hardening effect from bone. For error estimates of this technique, refer to Reference 6.

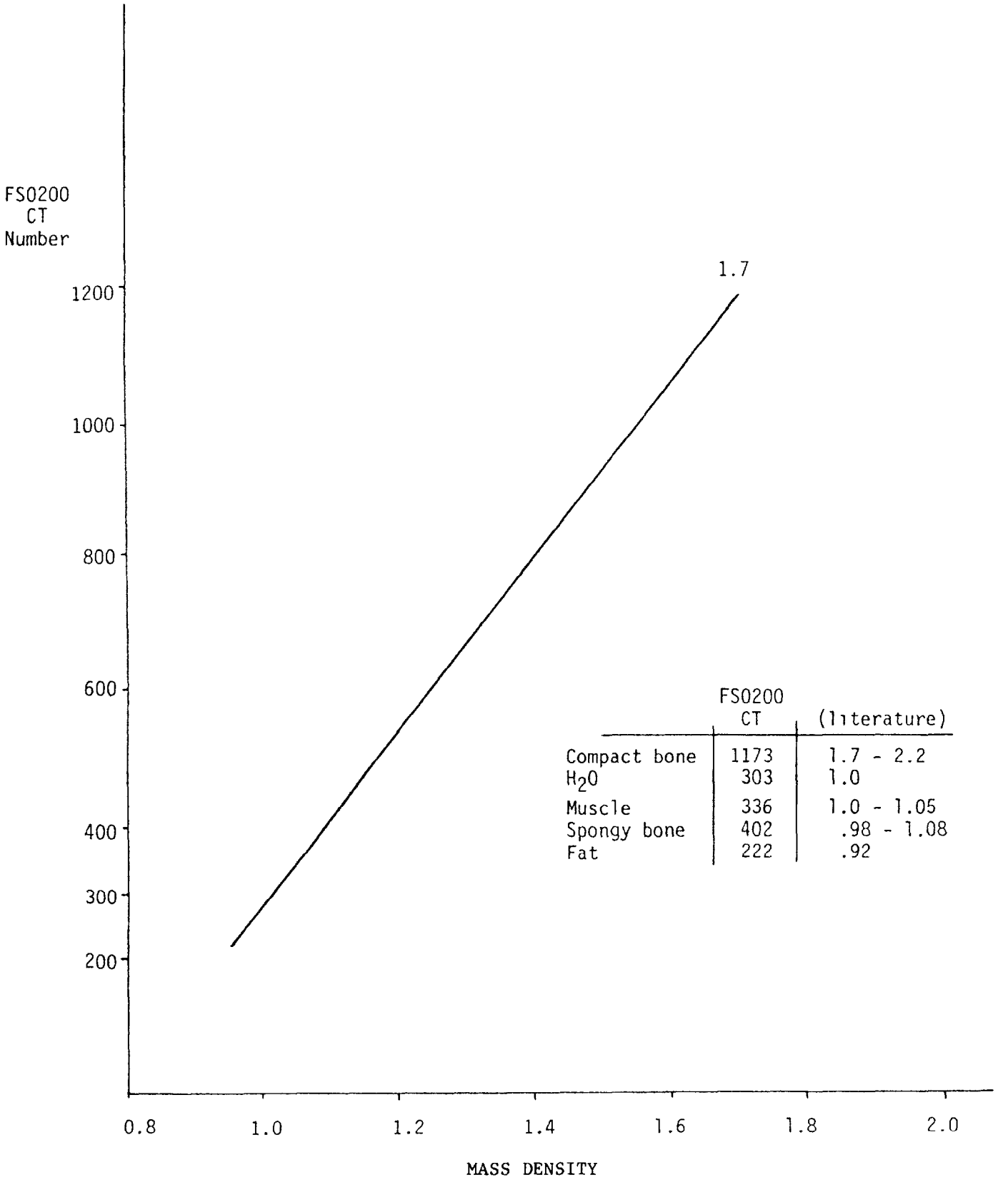

Figure D-4 A typical calibration curve for converting CT numbers to mass density.

2.2 Evaluation of Mass, Geometric Center, Center of Gravity, and Inertia Tensor of An Anatomical Structure

Mass Distribution

The mass of an anatomical structure in a cross section is calculated by integrating the structure's mass density over the entire volume in which it is contained. The volume may be contained in a few CT sections. The equation is in a discrete form since the geometric and mass density data are already in a digital format.

$$M = \left(\sum_{ijk} \rho_{ijk} \Delta V \right)$$

Where: M is the mass of an anatomical structure,

ρ_{ijk} is the mass density of the i,j pixel in section k, and

ΔV is the volume of each pixel.

The summation limits are determined from the coordinates of the outlines of the structure, while the mass density of each pixel is obtained from the CT numbers described in Section 4.2.1.

Center of Gravity

The center of gravity of section k of an anatomical structure is calculated by using the following equation:

$$\bar{x} = \sum \rho_{ij} x_i \Big/ \sum \rho_{ij}$$

$$\bar{y} = \sum \rho_{ij} y_j \Big/ \sum \rho_{ij}$$

$$\bar{z} = (1/2)\, z$$

Where x_i, y_j are the coordinates of pixel (i,j) and z is the z coordinate of section k.

Geometric Center

The geometric center (x_g, y_g, z_g) of a structure in a cross section is computed by using the maximum and minimum x and y coordinates x_{max}, x_{min}, y_{max}, y_{min} of the anatomical outline as follows:

$$x_g = (x_{max} + x_{min}) / 2$$

$$y_g = (y_{max} + y_{min}) / 2$$

$$z_g = (1/2)\ z$$

Inertia Tensor

The inertia tensor of the cross section k of an anatomical structure with respect to its center of gravity $(\bar{x},\bar{y},\bar{z})$ is computed from these equations:

$$I_{xx} = \sum_{ijk} \rho_{ijk} ((y - \bar{y})^2 + (z - \bar{z})^2)_{ijk} \Delta V$$

$$I_{yy} = \sum_{ijk} \rho_{ijk} ((x - \bar{x})^2 + (z - \bar{z})^2)_{ijk} \Delta V$$

$$I_{zz} = \sum_{ijk} \rho_{ijk} ((x - \bar{x})^2 + (y - \bar{y})^2)_{ijk} \Delta V$$

$$I_{xy} = I_{yx} = -\sum_{ijk} \rho_{ijk} ((x - \bar{x})\ (y - \bar{y}))_{ijk} \Delta V$$

$$I_{zy} = I_{yz} = -\sum_{ijk} \rho_{ijk} ((y - \bar{y})\ (z - \bar{z}))_{ijk} \Delta V$$

$$I_{zx} = I_{xz} = -\sum_{ijk} \rho_{ijk} ((x - \bar{x})\ (z - \bar{z}))_{ijk} \Delta V$$

SECTION E

ANATOMICAL GEOMETRY AND MASS DENSITY DISTRIBUTION DATA BASE

The following five types of data described in Section D from each cross section of a specimen have been saved:

1. Scan picture
2. Boundary coordinate
3. Anthropometric data
4. Boundary coordinates of internal organs
5. Anthropometric data of internal organs

These data are organized in three types of data file for each specimen:

1. Scan file
2. Boundary file
3. Anthropometric data file

The CT Scan File is the actual CT scan digital pictures. The Body Contour File consists of coordinates of anatomical structures extracted from CT scans. The Anthropometric Data File contains the area, mass, geometrical center, center of gravity and inertia tensor of all cross sections. Table E-1 shows the relationship among these Files using specimen 5 as an example.

At the present time all three types of files have been stored in 1600 BPI Master Tapes which can be read directly through PDP 11/34 RT-11 monitor PIP (Peripheral Interchange Programs) commands. In addition, contour files and anthropometric data files have been stored in the NHTSA (National Highway Treaffic Safety Administration) PDP 11/35 computer system. Data can be extracted by either copying onto a 800 BPI tape by using the RSX-11D operating system PIP or through telephone line time-sharing. The data format and the procedure of accessing these data will be described in Volume 2.

Table E-1 Relationship Among Three Types of Files

CT Scan File File Name	Contour File File Name	Anthropometric Data File File Name
SP05.001	SP5BN.001	SP5HD.001
SP05.011	SP5BN.011	SP5HD.011
.	.	.
.	.	.
SP05.341	SP5BN.341	SP5TO.341
.	.	SP5LA.341
.	.	SP5RA.341
.	.	.
SP05.621	SP5BN.621	SP5LL.621
.	.	SP5RL.621

BN: Boundary; HD: Head; TO: Torso; LA: Left Arm; RA: Rightt Arm; LL: Left Leg; RL: Right Leg.

As an example, Figure E-1 summarizes the data structure and the accessibility of the data.

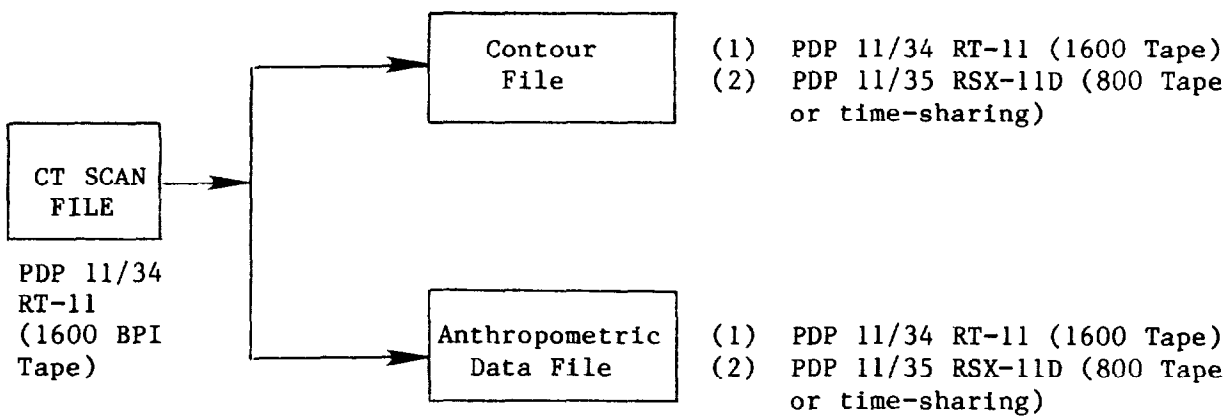

The data structure and contents of each specimen will be described in Volume 2.

Figure E-1 Data Structure of Specimen 5 and the Accessibility of the Data

SECTION F

GENERATION OF FINITE ELEMENT MESHES (13,14)

The discretization procedure and the generation of an internal mesh in two dimension and three dimension to be used for finite elements analysis of an anatomical component is discussed in this section. The basis of the discretization is the data obtained from the radiological computerized tomographic (CT) process discussed earlier in this report.

For each cross section, two arrays, $C_{y_{ob}}$ and $C_{y_{ib}}$ containing the coordinates of discrete points on the outer and inner boundaries of the internal organ from a scan are generated and stored. The generation of each of these arrays proceeds in such a way that for each value of y, in decreasing order, two values of x are found that define the coordinates of the two points on the boundary of the cross section. In addition to these arrays, for each cross section two other arrays $C_{x_{ob}}$ and $C_{x_{ib}}$ are formed containing the coordinates of each consecutive point on the outer and the inner boundaries of the cross section, proceeding in a clockwise direction.

During this process, the area A(I) of the internal organ in the section is also determined, as well as, the maximum and minimum values of the coordinates referred to as x_{max}, x_{min}, and y_{max}, y_{min}. The arrays of the coordinates form the basis of the development of the finite elements mesh, as outlined below.

1. Generation of Mesh for Cross Sections with No Internal Boundary (Cavity)

The steps to be followed are outlined below:

1) A typical cross section, referred to as the j-th cross section, is selected as the initial cross section to begin the mesh generation process for plane cross sections. As present, the cross section with the largest

or smallest z-coordinate is selected as the initial (j-th) cross section.

2) Starting with the j-th cross section a set of control points are established on the boundary.

Let

M_{ob} = Number of control points specified by the user for the outer boundary (presently M_{ob} is fixed as 12).

N_{ob} = Total number of points defining the outer boundary.

The first control point is chosen so as to coincide with the point having the maximum y-coordinate (i.e., y_{max}). The remaining control points are located in such a way as to sustain approximately equal arc lengths along the boundary curve. For this purpose an approximation to the perimeter of the boundary curve is obtained from

$$P = \sum_{i=1}^{N-1} ((x_{i+1} - x_i)^2 + (y_{i+1} - y_i)^2)^{1/2} + ((x_1 - x_{N_{ob}})^2 + (y_1 - y_{N_{ob}})^2)^{1/2} \quad (1)$$

Then the arc length, ℓ, between any two consecutive control points is approximately computed as:

$$\ell = P/M_{ob} \quad (2)$$

3) In locating each subsequent control point some minor adjustments are made to force the point to coincide with the closest boundary point in that neighborhood. Thus, starting with the initial control point, the second control point will obviously be located at a distance of $\ell_{I,II}$ which is obtained by accumulating a sufficient number of successive increments in chord lengths, namely

$$\ell_{I,II} = ((x_2 - x_1)^2 + (y_2 - y_1)^2)^{1/2} + ((x_3 - x_2)^2 + (y_3 - y_2)^2)^{1/2} + \ldots \quad (3)$$

As soon as the right-hand side of Eq. (3) becomes larger than ℓ (See Eq. 2), then the location of the second control point is chosen to coincide with the closest boundary point. To avoid cumulative errors, any small difference from the computed arc length is equally partitioned between the remaining arc lengths. Subsequent differences are dealt with in the same manner when locating the other control points.

4) The same procedure is used to locate the control points on the other cross sections. The first control point on each subsequent cross section is chosen to correspond to the point with the maximum y value. Alternatively, the first control point chosen as the distance between this point and the first control point of the preceding cross section is a minimum. This is accomplished in an appropriate manner by searching through the ordered array (C_y) for the cross section under consideration, and using x and y coordinates of each boundary point to define the distances of the points from the reference point (the first control point of the preceding cross section). The boundary point with the minimum distance is then labelled as the first control point of this cross section.

Ordinarily, the same number of control points will be used for all cross sections, although provisions will be made for specifying a different number of control points from cross section to cross section. Such an option can only be exercised if the finite element code that is used in the analysis of the internal organ contains transition elements in its element library.

5) For the purpose of generating the internal mesh, each cross section if initially considered as a single isoparametric quadrilaterial element and mapped into a square for the purpose of partitioning it into subregions. To this end, initially a set of twelve control points ($M_{ob} = 12$) is established on the outer boundary of each cross section. Thus, considering the j-th cross

section as defined previously, and starting with the first control point, four consecutive control points are selected constituting the first edge of the quadrilaterial region. Obviously, the first and fourth control points correspond to the corner nodes and the second and third to the intermediate nodes for an interpolating polynomial of order three.

Referring to Figure F-1.a, the first edge of isoparametric element is represented by the solid line joining the control points 1 through 4.

6) Continuing in this manner, the boundary line joining the next four control points corresponds to the second edge of the element, and so on. Thus, with reference to Figure F-1.a, the second edge is represetned by the doted line, the third by the solid - dotted line and the fourth by the dashed line.

The corresponding square in the integer square is shown in Figure F-1.b. the internal grid points in Figure F-1.b are the intersection points of the grid lines representing constant values of ξ and η, namely,

$\xi = \pm 1/3$ and $\eta = \pm 1/3$.

These grid lines are mapped into the section to create the curvilinear mesh that subdivides the cross section into nine subregions, as shown in Figure F-1.a.

For a cubic quadrilateral element, the shape Functions N_1 are generated from the following expressions corresponding to the corner and intermediate nodes, respectively.

$$N_1 = (1 + \xi\xi_i)(1 + \eta\eta_i)(9(\xi^2 + \eta^2) - 10)/32 \qquad (4)$$

$$N_i = 9(1 - \xi^2)(1 + 9\xi\xi_i)(1 + \eta\eta_i)/32 \text{ , for } \xi = \pm 1/3,\ \eta = \pm 1 \qquad (5)$$

$$N_i = 9(1 - \eta^2)(1 + 9\eta\eta_i)(1 + \xi\xi_i)/32 \text{ , for } \xi = \pm 1,\ \eta = \pm 1/3 \qquad (6)$$

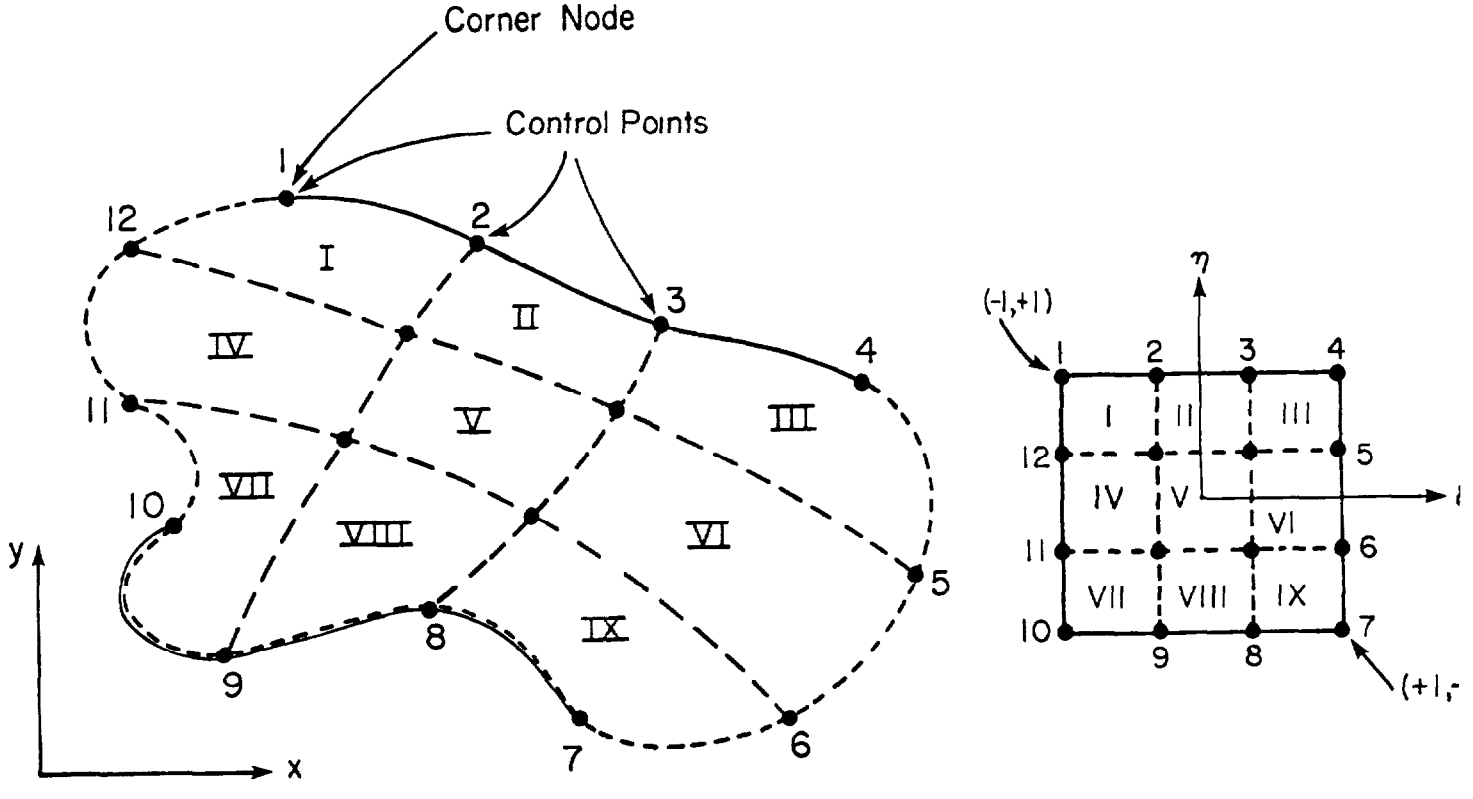

F-1.a A Typical Cross Section

F-1.b Transformed Shape

Figure F-1: A Typical Section Subdivided into Subregions

where ξ and η are the natural coordinates of the transformed element, and the ξ_i and η_i refer to the coordinates at the node points of the element.

Thus, in the case of Figure F-1, Eq. (4) is used for the corner nodes 1, 4, 7, and 10; Eq. (5) is used for control points 2, 3, 8, 9, and Eq. (6) is used for control points 5, 6, 11, 12. The coordinate system for the quadrilateral isoparametric element is the Cartesian x-y system. Based on the above shape functions the transformation between the two coordinate systems is defined as:

$$x = \sum_{i=1}^{12} N_i x_i \tag{7}$$

$$y = \sum_{i=1}^{12} N_i y_i \tag{8}$$

where x_i, y_i, are the corner nodes and control points depicted in Figure F-1.a.

7) Using the interactive computer graphics procedures, the particular cross section and its associated mesh is displayed for examination by the analyst. In case some distortion is observed in any of the subregions, some of the control points (usually not the corner nodes) can be relocated to remedy this situation.

8) Using the coordinates of the relocated points, the above steps are repeated to generate an improved set of subregions and internal mesh points for the cross section under consideration. This process is illustrated in Figures F-2 and F-3.

2. Generatation of Mesh for Cross Sections with Inner Boundary (Cavity) Present

When an inner boundary is present the above procedure can still be used with certain modifications. Thus, the first eight steps are followed as previously stated, and as a result j-th cross section is divided into nine

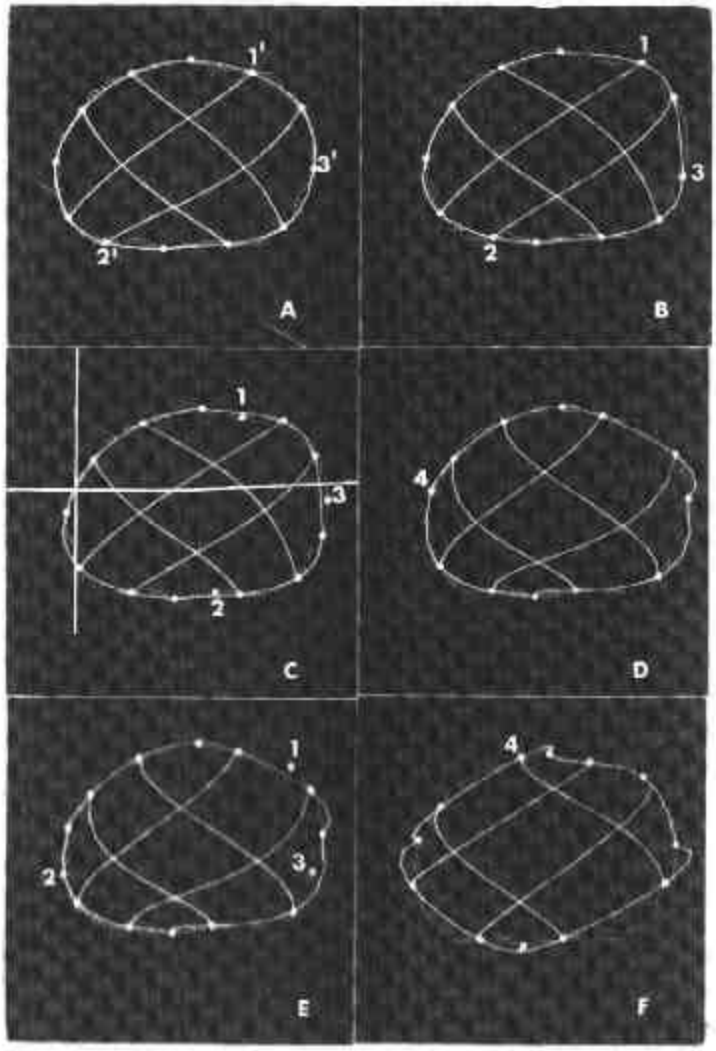

Figure F-2 After the initial internal mesh has been generated, it is possible for the user to modify the mesh through an interactive mode.

(a) The initial mesh
(b) The modified mesh after the user relocates three control points (1',2',3') to (1,2,3).
(c) The user plans to relocate four control points again on (b). It can be done by moving a cursor (two white cross lines) through the boundary, three new control points have been relocated so far (1,2,3).
(d) After the 4th point (4) has been relocated, the program generates a new internal mesh [compare (c) and (d)].
(e) The user wants to relocate four more control points on (d). Three points have been done (1,2,3) so far.
(f) The modified mesh from (e) after the 4th control point is relocated (4) [compare (e) and (f)]. Compare the drastic differences between the mesh shown in (a) and (f).

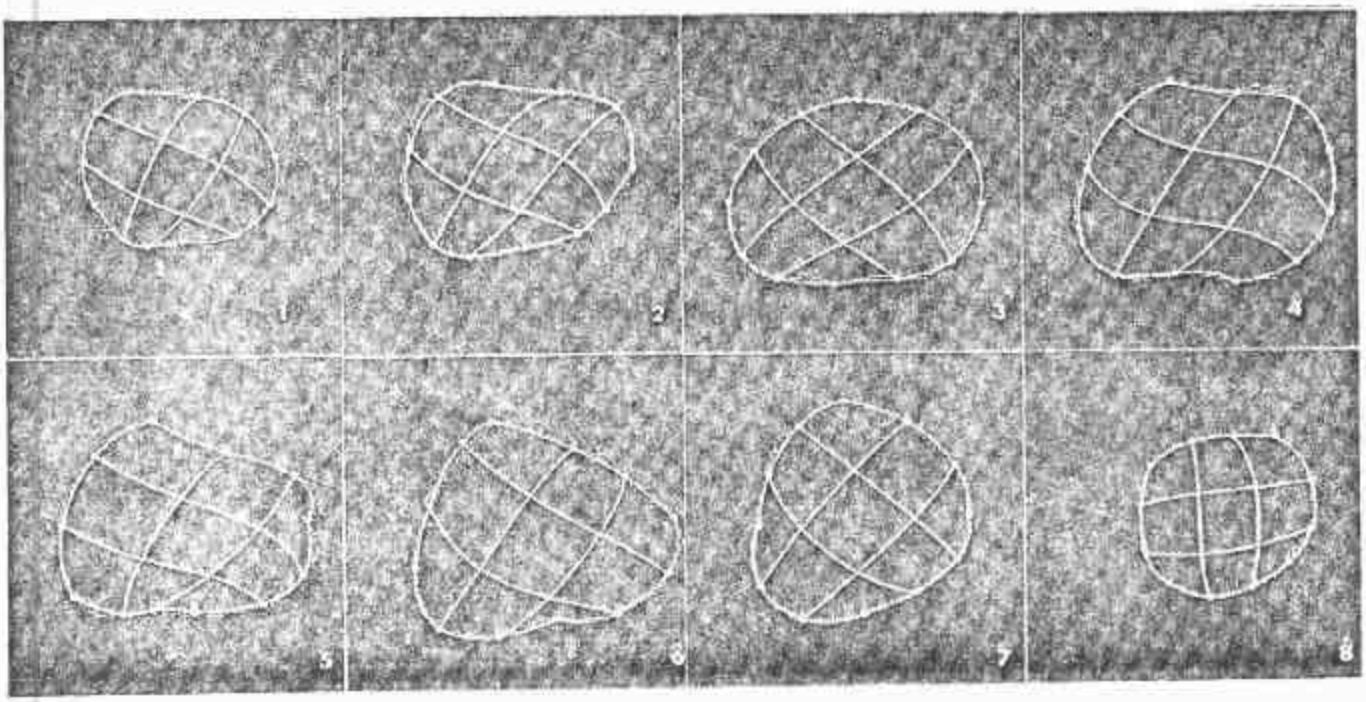

Figure F-3 Internal mesh of eight cross sections through the heart. The display scale used for each cross section is based on the maximum and minimum values of the x and y coordinates of that section. The original outlines from scan pictures are shown in the dotted lines. The solid lines are the computer generated smoothed boundaries and the internal meshes.

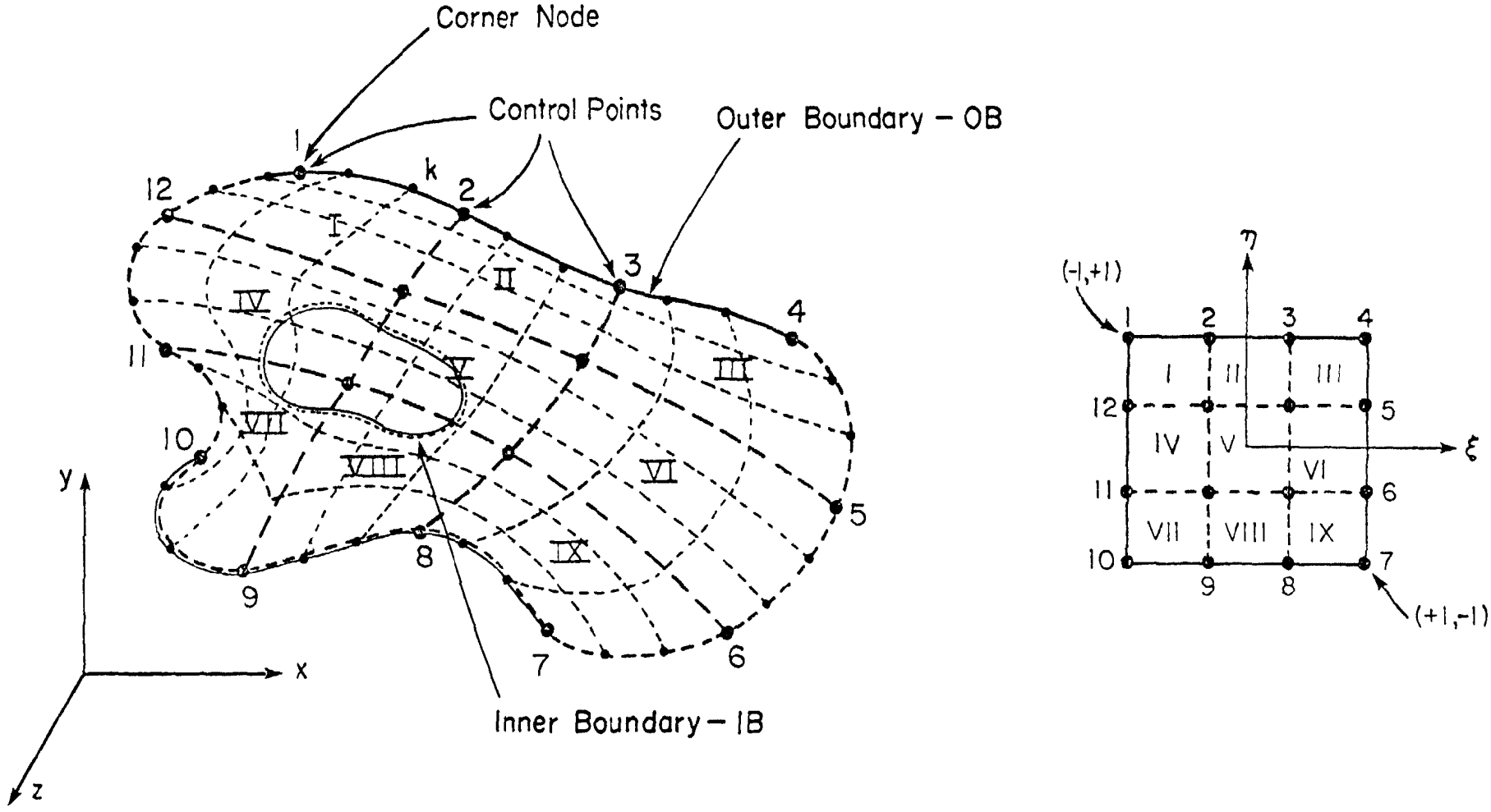

Figure F-4 A Section with an inner cavity or region of different material properties.

subregions as indicated in Figure F-4. The remaining steps are outlined below:

9) As shown in Figure F-4, the inner boundary is designated as the subregion IB. As discussed previouly, the array $(C_x)_{ib}$ containing the coordinates of the discrete points of the boundary IB and the maximum and minimum values of the coordinates, i.e., x_{max}, x_{min}, and y_{max}, y_{min} are known. These extreme values can be used as bounds for determining whether a certain grid line passes through IB. Thus, for example, if a grid line corresponding to ξ = constant is mapped onto the physical space by selecting closely spaced values of η from +1 to -1, a typical grid line such as k-ℓ with the inner boundary curve can be found by means of Eqs. (7) and (8). The intersection points, or as a special case the point of tangency, of k-ℓ with the inner boundary curve can be found approximately by taking small increments in η as the inner boundary is approached and locating the intersection point approximately by finding the closest discrete point on the inner boundary using array $(c_x)_{ib}$. The second intersection point on the other side of the boundary curve is found in a similar manner.

10) For a grid line along η = constant, the same process can be repeated to determine the intersection points with the inner boundary.

11) As may be seen from Figure F-4, the presence of the internal boundary causes the neighboring elements to be split up into more elements, to distinguish between elements inside or outside of IB.

Referring to Figure F-4, the intersection points of two successive grid lines with the inner boundary together with the respective segment of the boundary constitute one of the edges of the associated elements. Such intersection points are to be considered as control points for the inner boundary. Some of the sub-elements may possess either three or five edges

(sides), instead of the conventional four.

Thus, referring to Figure F-4, this may occur near either end of the inner boundary. In such a case, the sub-element inside the inner region possesses three edges and the sub-element outside five edges. In the former case one of the edges may simple be subdivided into two parts by the introduction of an additional intermediate node point, leading to the normal four-edged element. However, in the latter case two of these edges may be combined together and considered as a single edge, of the interpolation processes involved in the finite element analysis would be reduced. Instead, it would be more effective to introduce an additional node on the inner boundary curve and further subdivide the sub-element into two sub-elements. This can be accomplished analytically as follows:

a. The elements that fall into this category are detected determining the last regularly spaced grid line corresponding to the ξ-direction that intersects the inner boundary at two points. The coordinates of both these intersection points are determined as previously explained.

b. Likewise, in the vicinity of the inner boundary, the last grid line corresponding to the η-direction is determined.

c. Considering the grid lines in the two directions and the segment of the inner boundary between the grid lines, an additional node point is introduced near the midpoint of the segment.

d. The node point can in most instances be joined with the exterior intersection point of the two adjacent grid lines to subdivide the exterior sub-element into two sub-elements.

If the resulting sub-elements do not possess acceptable shapes within a desired degree of regularity, then the additional node point is relocated using interactive graphic techniques to improve the shape of the sub-elements.

Alternatatively, the exterior intersection point of the adjacent grid lines may be relocated to improve the shape of the elements.

3. Generation of the Three-Dimensional Mesh for an Internal Organ

The extension of the two-dimensional case to the generation of a three-dimensional mesh for an internal organ is rather straightforward. The body is initially subdivided into a set of coarse subvolumes represented by three-dimensional isoparametric elements of a specific order (usually quadratic or cubic). Each of these elements is associated with a cube in the integer space for the purpose of generating subsequently a finer mesh for each of the subvolumes of the internal organ. The steps to be followed in the subdivision of the body into subvolumes and establishing the coarse three-dimensional mesh is outlined below.

1) Beginning with the j-th cross section, each subregion is considered to constitute an end surface (face) of a three-dimensional isoparametric element, for a total of nine such elements. For an element of cubic order two intermediate nodes need be established on each edge of the subregion. This is accomplished easily using the previously defined interpolation functions. However, in order to maintain as high an accuracy as is practically possible, in the case of points near the outer boundary these points are relocated to coincide with the closest discrete points that were originally generated from the scanning process stored in array ($C_{x_{ob}}$).

If an element of quadratic order is used then only one intermediate node need be determined on each side of the element.

2) In order to complete the definition of each isoparametric element, corresponding points are included from the associated subregions of cross sections j + 1, j + 2, j + 3. If successive cross sections are spaced too closely, some of the cross sections are skipped in order to maintian the

proper aspect ratios of the elements.

3) This is repeated for similar groupings of cross sections for the remaining sections preceding and following the j-th cross section. In this manner a set of coarse three-dimensional hexahedral elements is generated spanning the entire body (anatomical component).

4) Using isoparametric element concepts, each hexahedral element is mapped into a cube. This is represented by Figure F-5, which indicates the numbering scheme used for a cubic element with 32 nodes. The shape functions for each group are given.

a. Corner Nodes

Nodes i = 1, 4, 7, 10, 14, 16, 19, 22: $\xi = \pm 1$, $\zeta = \pm 1$

$$N_i = (1 + \xi\xi_i)(1 + \eta\eta_i)\left[1 + \zeta\zeta_i\right)\ (9(\xi^2 + \eta^2 + \zeta^2)-19)/64 \qquad (9)$$

For example, the above function at nodes 4 and 7 takes the form of:

$\underline{i = 4}$: $\xi_i = +1$, $\eta_i = +1$, $\zeta_i = +1$

$$N_4 = (1 + \xi(1)) + (1 + \eta(1))(1 + \zeta(1))\ \ (9(\xi^2 + \eta^2 + \zeta^2-19))/64 \qquad (10)$$

Or

$$N_4 = (1 + \xi)(1 + \eta)(1 + \zeta)\ (9(\xi^2 + \eta^2 + \zeta^2)-19)/64 \qquad (11)$$

Obviously, the same function should assume the value of unity if evaluated at point 4 (see Figure F-5), thus

$$N_{4/4} = (1 + 1)(1 + 1)(1 + 1)(9(1 + 1 + 1)-19) = (8)(8)/64 = 1 \qquad (12)$$

$\underline{i = 7}$: $\xi_i = +1$, $\eta_i = -1$, $\zeta_i = +1$

$$N_7 = (1 + \xi)(1 - \eta)(1 + \zeta)\ (9(\xi^2 + \eta^2 + \zeta^2)-19). \qquad (13)$$

Likewise, evaluating the above function at node 7.

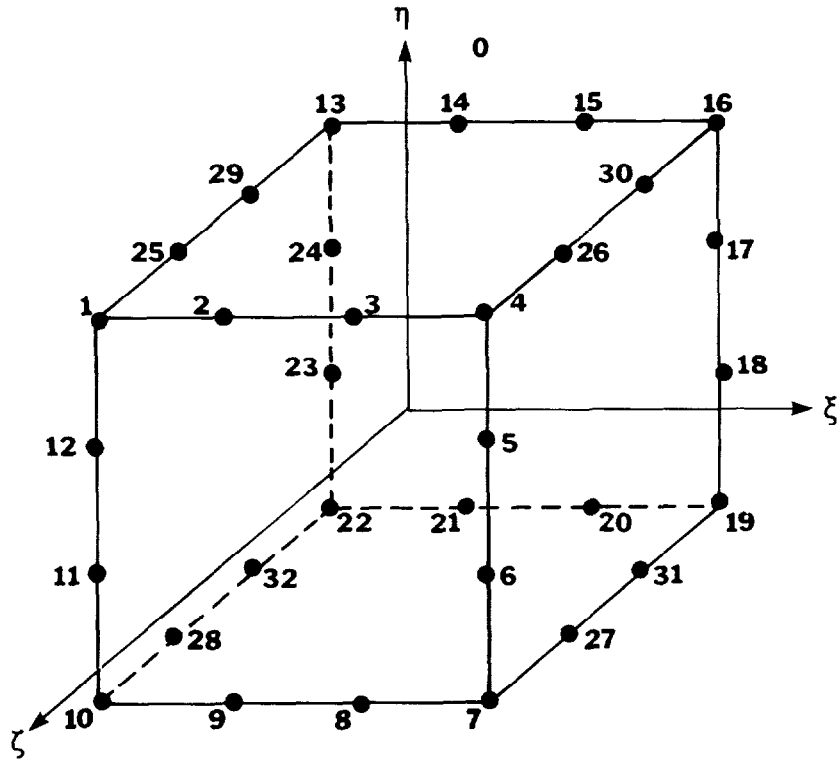

Figure F-5 Transformed Shape of Isoparametric Hexahedral Element in Integer Space

$$N_{7/7} = (1 + 1)(1 - (-1))(1 + 1)(9(1 + 1 + 1) - 19)/64 = 1 \quad (14)$$

b. Intermediate Nodes on Edges $\eta = +1$, $\xi = \pm 1$

Nodes $i = 25, 26, 29, 30$

$$N_i = 9(1 - \zeta^2)(1 + 9\zeta\zeta_i)(1 + \xi\xi_i)(1 + \eta\eta_i)/64 \quad (15)$$

Considering nodes 25 and 30 in this group:

$\underline{i = 25}$: $\xi_i = -1$, $\eta_i = +1$, $\zeta_i = +1/3$

$$N_{25} = 9(1 - \zeta^2)(1 + 3\zeta)(1 - \xi)(1 + \eta)/64 \quad (16)$$

$\underline{i = 30}$: $\xi_i = +1$, $\eta_i = +1$, $\zeta_i = 1/3$

$$N_{30} = 9(1 - \zeta^2)(1 - 3\zeta)(1 + 3\xi)(1 + \eta)/64 \quad (17)$$

c. Intermediate Nodes on Edges $\eta = -1$, $\xi = \pm 1$

Node $i = 27, 28, 31, 32$

$$N_i = 9(1 - \zeta^2)(1 + 9\zeta\zeta_i)(1 + \xi\xi_i)(1 + \eta\eta_i)/64 \quad (18)$$

Considering nodes 31 and 28 in this group:

$\underline{i = 31}$: $\xi_i = +1$, $\eta_i = -1$, $\zeta_i = -1/3$

$$N_{31} = 9(1 - \zeta^2)(1 - 3\zeta)(1 + \xi)(1 - \eta)/64 \quad (19)$$

$\underline{i = 28}$: $\xi_i = -1$, $\eta_i = -1$, $\zeta_i = 1/3$

$$N_{28} = 9(1 - \zeta^2)(1 + 3\zeta)(1 - \xi)(1 - \eta)/64 \quad (20)$$

d. Intermediate Nodes on Edges $\eta = +1$, $\zeta = \pm 1$

Nodes $i = 2, 3, 14$, and 15

$$N_i = 9(1 - \xi^2)(1 + 9\xi\xi_i)(1 + \eta\eta_i)(1 + \zeta\zeta_i)/64 \quad (21)$$

Considering nodes 15 and 2 in this group:

i = 15: $\xi_i = +1/3$, $\eta_i = +1$, $\zeta_i = -1$

$$N_{15} = 9(1 - \xi^2)(1 + 3\xi)(1 + \eta)(1 - \zeta)/64 \quad (22)$$

i = 2: $\xi_i = -1/3$, $\eta_i = +1$, $\zeta_i = +1$

$$N_2 = 9(1 - \xi^2)(1 - 3\xi)(1 + \eta)(1 + \zeta)/64 \quad (23)$$

e. Intermediate Nodes on Edges $\eta = -1$, $\zeta = \pm 1$

Nodes i = 9, 8, 20, 21

$$N_i = 9(1 - \xi^2)(1 + 9\xi\xi_i)(1 + \eta\eta_i)(1 + \zeta\zeta_i)/64 \quad (24)$$

Considering Nodes 21 and 8 in this group:

i = 21: $\xi_i = -1/3$, $\eta_i = -1$, $\zeta_i = 1$

$$N_{21} = 9(1 - \xi^2)(1 - 3\xi)(1 - \eta)(1 - \zeta)/64 \quad (25)$$

i = 8: $\xi_i = +1/3$, $\eta_i = 1$, $\zeta_i = +1$

$$N_8 = 9(1 - \xi^2)(1 + 3\xi)(1 - \eta)(1 + \zeta)/64 \quad (26)$$

f. Intermediate Nodes on Edges $\xi = +1$, $\zeta = \pm 1$

Nodes i = 5, 6, 17, and 18

$$N_i = 9(1 - \eta^2)(1 + 9\eta\eta_i)(1 + \xi\xi_i)(1 + \zeta\zeta_i)/64 \quad (27)$$

Considering Nodes 5 and 18 in this group:

$\underline{i = 5}$: $\xi_i = +1,\ \eta_i = +1/3,\ \zeta_i = +1$

$$N_5 = 9(1 - \eta^2)(1 + 3\eta)(1 + \xi)(1 + \zeta)/64 \tag{28}$$

$\underline{i = 18}$: $\xi_i = +1,\ \eta_i = -1/3,\ \zeta_i = -1$

$$N_{18} = 9(1 - \eta^2)(1 - 3\eta)(1 + \xi)(1 - \zeta)/64 \tag{29}$$

g. Intermediate Nodes on Edges $\xi = -1,\ \zeta = \pm 1$

Nodes i = 11, 12, 23, 24

$$N_i = 9(1 - \eta^2)(1 + 9\eta\eta_i)(1 + \xi\xi_i)(1 + \zeta\zeta_i)/64 \tag{30}$$

Considering Nodes 24 and 11 in this group:

$\underline{i = 24}$: $\xi_i = 1,\ \eta_i = +1/3,\ \zeta_i = 1$

$$N_{24} = 9(1 - \eta^2)(1 + 3\eta)(1 - \xi)(1 - \zeta)/64 \tag{31}$$

$\underline{i = 11}$: $\xi_i = 1,\ \eta_i = 1/3,\ \zeta_i = +1$

$$N_{11} = 9(1 - \eta^2)(1 - 3\eta)(1 - \xi)(1 + \zeta)/64 \tag{32}$$

In the development of the computer algorithm, it is more convenient to classify the above functions into a group of four general functions as shown below:

For $\xi = \pm 1,\ \eta = \pm 1,\ \zeta = \pm 1$

$$N_i = (1 + \xi\xi_i)(1 + \eta\eta_i)(1 + \zeta\zeta_i)[9(\xi^2 + \eta^2 + \zeta^2) - 19]/64 \tag{33}$$

For $\xi = \pm 1/3,\ \eta = \pm 1,\ \zeta = +1$

$$N_i = 9(1 - \xi^2)(1 + 9\xi\xi_i)(1 + \eta\eta_i)(1 + \zeta\zeta_i)/64 \tag{34}$$

For $\eta = \pm 1/3$, $\xi = \pm 1$, $\zeta = \pm 1$

$$N_i = 9(1 - \eta^2)(1 + 9\eta\eta_i)(1 + \xi\xi_i)(1 + \zeta\zeta_i)/64 \quad (35)$$

For $\zeta = \pm 1/3$, $\xi = \pm 1$, $\zeta = \pm 1$

$$N_i = 9(1 - \zeta^2)(1 + 9\zeta\zeta_i)(1 + \xi\xi_i)(1 + \eta\eta_i)/64 \quad (36)$$

It should be noticed that Eqs. 4-6 are special cases of the above equations, and thus in the software package only Eqs. 33-36 are implemented.

5) Having subdivided the anatomical component into subvolumes, the discretized system is displayed graphically and improvements are performed, if necessary, on the original mesh by relocating certain node points either by analytical means or interactive graphic processes. Also, in case there are user specified control points marking a physical separation curve, joint, etc., care is exercised to locate some of the node points near several of such control points.

6) The three-dimensional coarse mesh developed in this manner forms the basis of subdividing the anatomical component into a finer mesh as specified by the analyst. However, the above procedure applies to the case where the anatomical component does not posses an internal region and associated boundary surface is present, the above procedure must be modified as indicated below.

7) Considering each cross section affected by the presence of the inner region, the intersection of the grid lines with the inner boundary is determined as explained previously in the treatment of 2-D planar cross sections with inner boundary present. Likewise, the elements spanning over the inner boundary are split up into subelements spanning over the inner boundary are split up into subelements that are entirely interior and exterior to the

inner boundary as indicated in detail previously. Obviously, such subdivision affects the associated three-dimensinal isoparametric element that span from cross section to cross section.

8. For those isoparametric elements commmon to the outer and inner regions, possible intersections of grid lines in the z direction must be investigated. This may lead to further splitting of elements, in a three-dimensional sense, in order to distinguish between elements in the interior and exterior of the inner boundary (cavity) surface.

Software Development - Based on the aforementioned algorithms, a software package for 2 and 3 dimensional mesh generation has been developed. The software package is divided into two distinct categories:

1) Software for graphical display of mesh and bodies;

2) Software for generation of data to be used as input to the display package.

The software for graphical display is a set of subroutines that interface the TEKTRONIX Terminal Control System either directly (for 2-D displays) or through an implementation of the CORE Graphics Standard System. The CORE system is a software package that incorporates the facilities for graphic view transformation in 2-D and 3-D. Also, this system is used to display the 3-dimensional mesh. The interface to this package consists of subroutines FIGURE, DREGN, and DFMSH. The following is a description of these subroutines.

(1) Subroutine FIGURE. This subroutine is used to set up the viewing parameters utilized in the CORE system. These parameters are the viewing direction, viewing distance, type of projection (i.e., parallel or perspective), location of projection point windowing information, viewport data, viewing volume and flags for enabling clipping facilities. Definition of some of thse parameters are given in Figure F-6. A more comprehensive

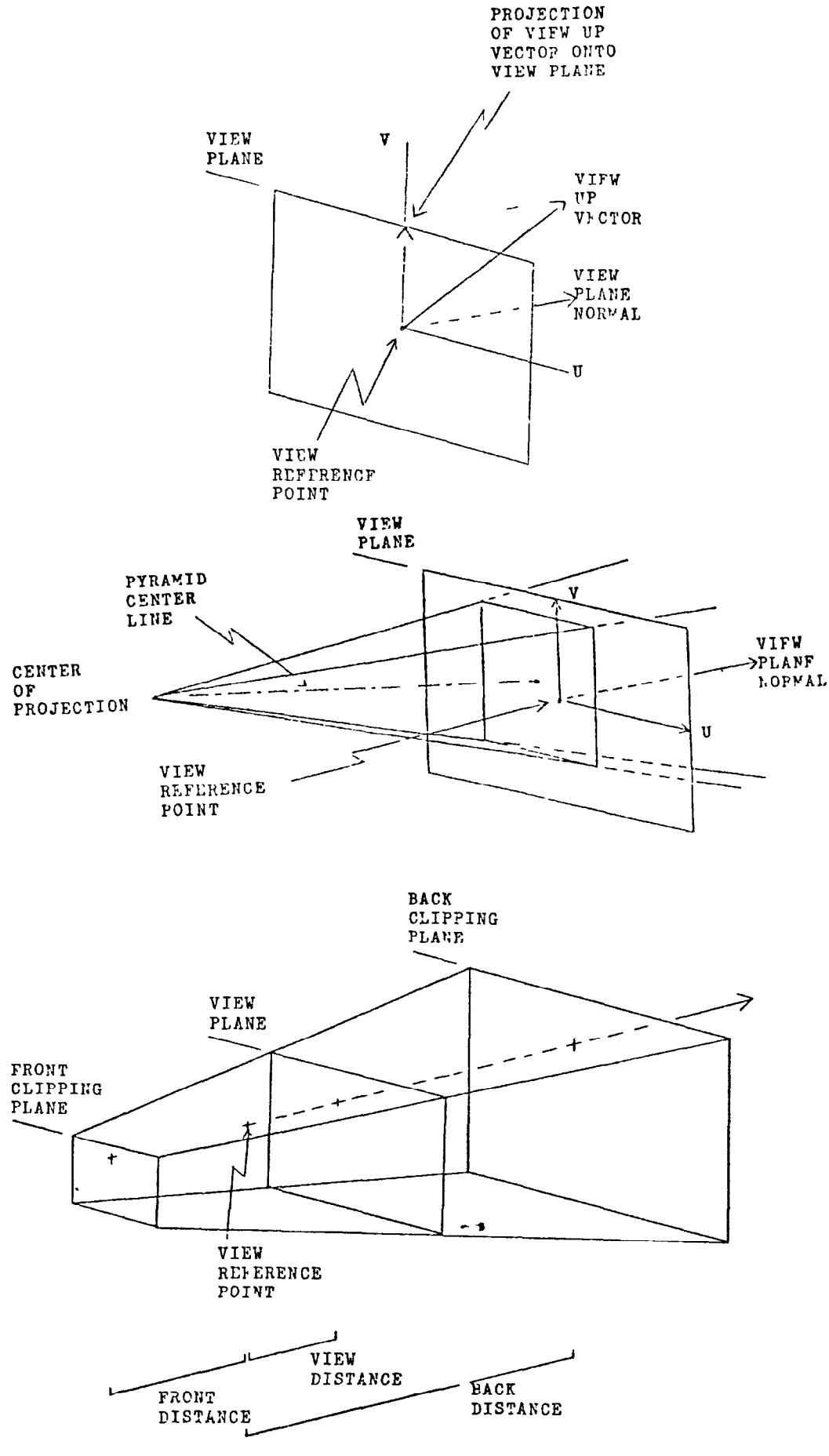

Figure F-6 Definition of Viewing Transformation Parameters

definition can be found in Reference (15).

(2) Subroutine DREGN. This subroutine is used to display a designated portion of the coarse mesh. The input to this subprogram consists of the region number IDR; the array IREG, listing the 32 nodes defining each region; and the array COORD, which contains the x, y, and z coordinates of all the node points previously generated. The subroutine then generates the needed graphical data by utilizing a series of move and draw commands (i.e., calling subprograms MARKA3 and PLINA3, respectively, of the CORE system to display the region of interest.

(3) Subroutine DFMSH. This subroutine is parallel to the subroutine DREGN and is used to display the mesh within each of the regions defined in the initial coarse subdivision.

The two-dimensional graphic display package is parallel to the subroutine DREGN and is used to display the mesh within each of the regions defined in the initial coarse subdivision.

(1) Subroutine DINIT. This subroutine is used to initialize the terminal control system and to define the 2-dimensional window and viewport. This is accomplished through the input values of XMIN, XMAX, YMIN, and YMAX which represent the extreme values that define a given cross section of the x and y coordinates of points.

(2) Subroutine DBOUND. This subroutine is used to display the digitized points defining the given cross section. In displaying the boundary points the subprogram skips the designated number of points. This subprogram is used to display the boundary of both the outer and the inner boundary points.

(3) Subroutine DCTL. This subprogram is used to indicate the location of the 12 control points for a given cross section by drawing circles with a user defined radius centered at each of the 12 contol points. Subroutine

CIRCLE is used for this latter purpose.

(4) Subroutine DMESH. This subprogram displays the coarse mesh within each cross sectin. The main input data to this subprogram consists of the array COORD which lists the x, y, and z coordinates of all nodes generated at this time, nodes so far generated noted, and array COINT defining the integer space coordinates.

(5) Subroutine MODMSH. This subroutine is used to interactively modify the location of the control points within each cross section, if the user so desires. The subroutine allows the redefinition of up to 12 control points and uses the graphic cursor (cross hair) position reading facility of the 4010 series TEKTRONIX terminals. This subprogram utilizes the two auxiliary subroutines CIRCLE, as described before, and CROSS which draws an x to indicate the location of the deleted control point.

The software corresponding to Category II is used to process the input data pertaining to individual cross sections. This is to define the original 12 control points for each cross section and the redefinition of these at the option of the user, and to generate the initial 3-dimensional coarse mesh and the final mesh data to be used in the display package. The following subroutines are classified under this category.

(1) Subroutine READ. This subroutine is used to read the digitized data defining a given cross section. On return, the subroutine provides the array CX listing the x and y coordinate pairs, the total number of coordinate pairs N, the extrenum values of the x and y coordiantes XMIN, XMAX, YMIN, YMAX and the quantity XYMAX which is the x coordinate of the point with maximum y coordinate YMAX.

(2) Subroutine CNTLPT. This subroutine determines the 12 control points for each cross section by locating the 12 points such that the arc length

between each pair is almost the same and is equal to 1/12 of the total arc length of the boundary. The first control point is always taken as the point with maximm y coordinate, i.e., coordinates XYMAX, YMAX. This subroutine utilizes an auxiliary subprogram function CLEN which provides the facility for determining the approximation to the curve length of a segment of the boundary defined by two points located at the extremums of the segment.

(3) Subroutine MODCTL. This subroutine handles the updating of the list of the control points for a cross section if the user has modified the original control points through interaction with the software package. For a given cross section the x and y coordinates of the points designated in subroutine MODMSH are passed to this subroutine as input. MODCTL then searches the CX array to determine the point on the boundary that is closest to the control point under consideration. Once such a point is found, the coordinates of the newly determined point are substituted for the coordinates of the given control point. The determination of the closest point is done through utilization of subroutine SDIST.

(4) Subroutine UPCONT. This subprogram updates the array COORD (i.e., the list of the x, y, and z coordinates of the generated nodes), once the location of the control points for the cross section has been finalized. The one dimensional array COORD is set up to contain the coordinates x,y, and z for all points refering to the cross sections and the coarse 3-D mesh. The data in this array is stored sequentially and has the following format:

	1	2	3	4	5	6	
I							
	x_1	y_1	z_1	x_2	y_2	z_2	....
COORD (I)							
	point 1			point 2			

(5) Subroutine INGRID. Having mapped the boundary of a cross section into a unit square, the coordinates of the 4 interior points corresponding to the intersections of the grid lines for the coarse mesh is determined by subroutine INGRID through isoparametric transformation given by Eqs. 4-8.

(6) Subroutine FNDXYZ. This subroutine determines the real x,y, and z coordinates of a given point if its integer space coordinates, as well as the real coordinates of the control points, define the subregion that the given point lies is specified. This subroutine utilizes the shape functions given in Eqs. 33-36.

(7) Functions FNC, FNS, FNT, FNR. These functions are the implementations of the shape functions given in Eqs. 33-36, respectively.

(8) Subroutine INICO. The mapping of the organ into a cube or series of cubes requires the definition of 32 node (control) points and their integer space coordinates. The definition of the integer space coordiantes of the points defined in Figure F-5 is done by subroutine INICO which generates the one-dimensional array COINT. The following is the data format for this array.

	1	2	3	4	5	6		96
I								
COINT (I)	ξ_1	η_1	ζ_1	ξ_2	η_2	ζ_2	....	ζ_{32}
	boundary point 1			boundary point 2				

(9) Subroutine GSDCNT. Consistent with the two-dimensional case the body must be subdivided into 27 three-dimensional elements, each having its own 32 control points as seen in Figure F-7. In this figure, the information pertaining to 64 of the required points are known from the processing of the cross sections. These are shown in Figure F-7 and correspond to the control points defining the 9 regions of a given cross section. The

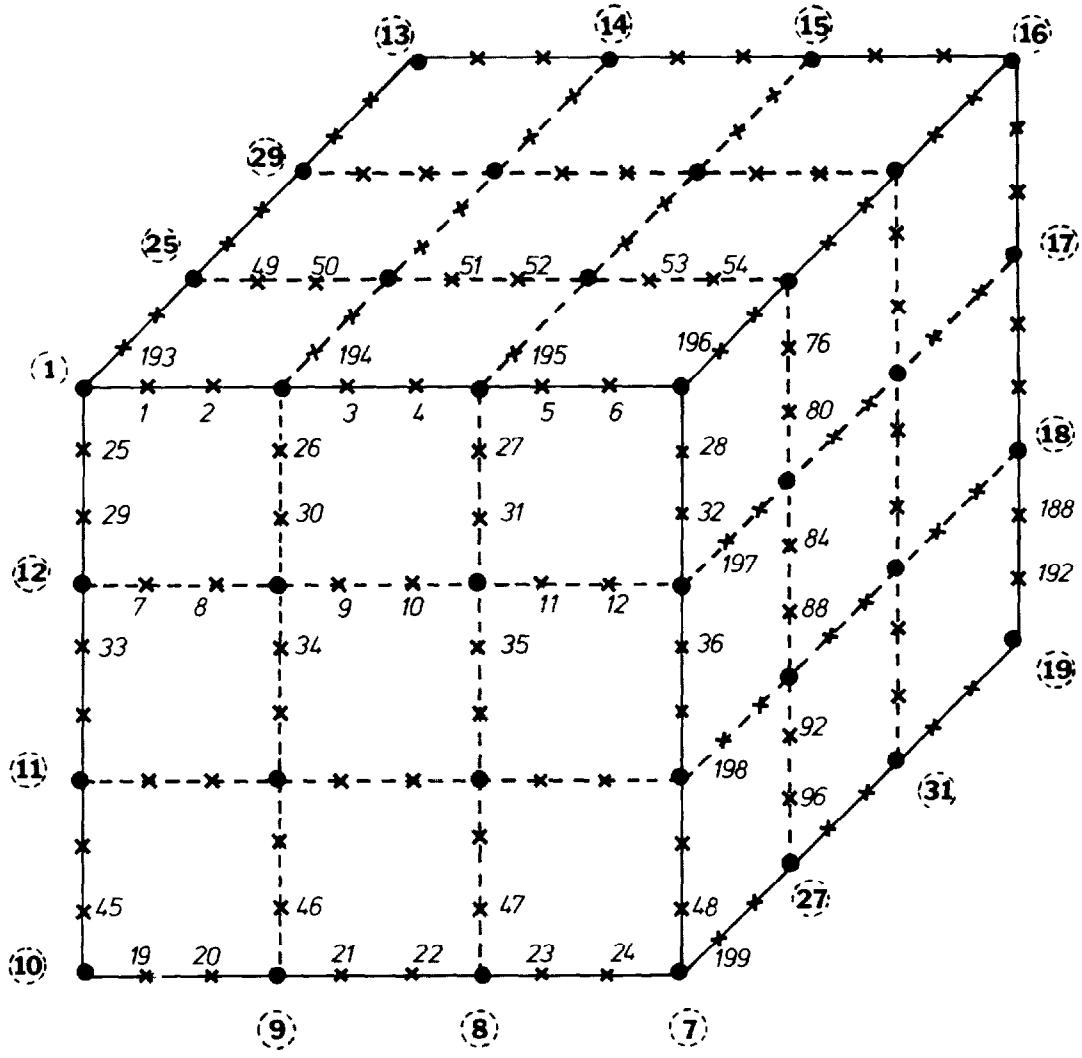

Figure F-7 Numbering Convention for Intermediate Points Defining a Subregion

X Intermediate point

• Control points defined for a cross section

) Control point numbering (See Figure F-5)

coordinates of the other 264 points (shown in Figure F-7 by x mark) are then obtained by utilizing the shape function given in Eqs. 33-36. Subroutine GSDCNT generates the integer space coordinates of these intermediate points and places them in the linear array.

SDCONT. The storage format of data in this one dimensional array is as follows:

I	1	2	3	4	5	6	----	
	ξ_1	η_1	ζ_1	ξ_2	η_2	ζ_2		ζ_{264}
SDCONT (I)	Intermediate Point 1			Intermediate Point 2				

It should be pointed out that arrays COINT and SDCONT are generated only once since the data is not volatile.

(10) Subroutines PRELIM and INTER. These two subprograms are used to define the coarse three dimensional mesh by filling the linear array IREG. This array contains the list of points defining a subregion. For each subregion the arrangement of point numbers correspond to the definition in Figure F-5. The data is arranged as follows:

I	1	2	3	32	33	
IREG(I)	1st point	2nd point	3rd point	32 point	1st	....
	Subregion 1				Subregion 2	

The final 3-D mesh for a given subregion is determined by utilization of subroutines SPLIT, FNDCRNS, and NODENUM. The description of these subprograms is as follows:

(11) Subroutine SPLIT. This subprogram accepts the mesh size parameters and directs the generation of the final mesh. It allows the subdivision of a regular region (one of the subregions in the coarse mesh) or any portion of the body. The latter facility requires the input of the integer space coordinates of the 8 nodes defining the corners of the desired subregion in

the integer space. This subroutine generates three linear arryas SCOORD, PCOORD, and ELEM. The structure and the format for data in these linear arrays are the same as the linear arrays COINT, COORD, and IREG, respectively, except that they refer to the final mesh.

(12) Subroutine FNDCRNS. This subprogram determines the coordinates of the corners of a subregion once the subregion number is defined. This data is then passed to subroutine SPLIT through array XNUM for subsequent processing.

(13) Subroutine NODENUM. This subprogram is the counter part for subroutine PRELIM and INTER as discussed before. In this subroutine the integer array ELEM is filled with data defining the node points for the 3-D final mesh. When an inner boundary is present, additional processing of data is needed. The subroutines NEWPNT, FNDCPIB, HORIZ, VERT, SEARCH, and MID are utilized to generate the required data. The description of these software is as follows:

(14) Subroutine NEWPNT. When referring to Figure F-8, it is desirable to determine whether a certain grid line such as k-1 passes through the inner boundary IB. To check for this, additional points on each grid line have to be determined. The points on the grid line corresponding to the coarse mesh are already known. These are designated by x marks in Figure F-8. The other points, i.e., the four interior points in each of the subregions 1 through 9 are then found by subroutine NEWPNT which calculates the real (x, y, and z) and the integer space coordiantes of these points. The real coordinates are stored in array COORD and the integer space coordinates are saved in array NPNTS. The data structure and the numbering scheme are shown in Figure F-9.

(15) Subroutines FNDCPIB, MORIZ, and VERT. The determination of the intersection points of the grid lines with the inner boundary is done by subroutine FNDCPIB. This program in turn calls subroutines HORIZ, VERT, and

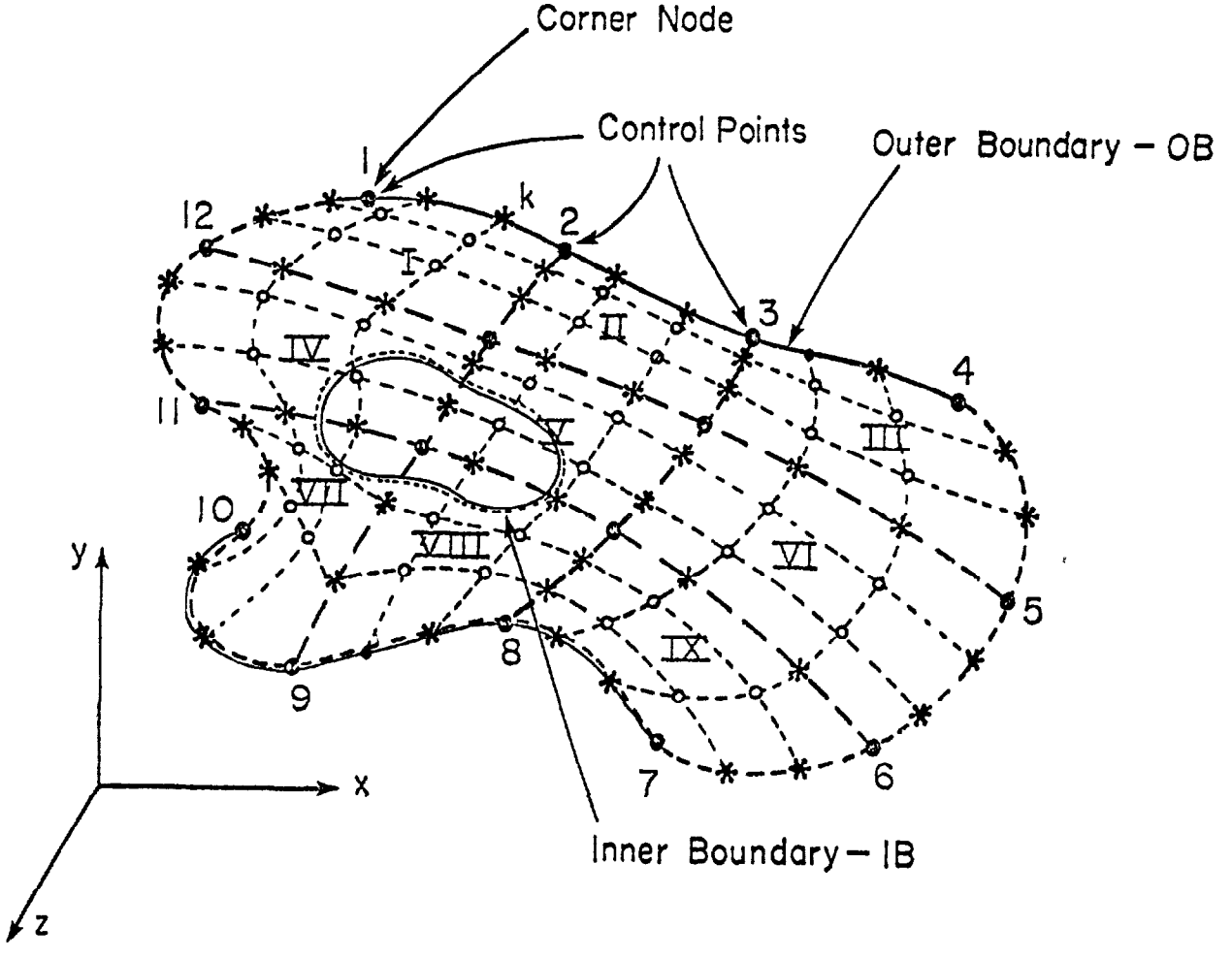

Figrue F-8. A Cross Section with Inner Boundary Present

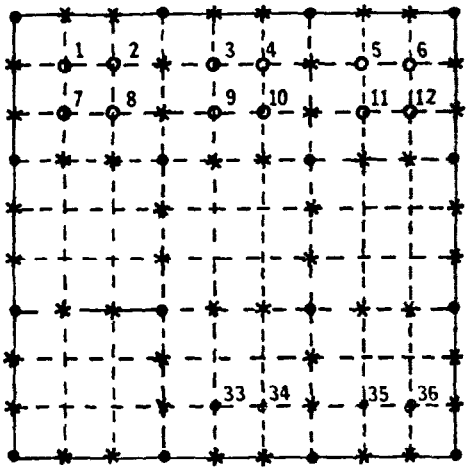

• Original Control Points

* Auxiliary Points

° Points Processed by NEWPNT

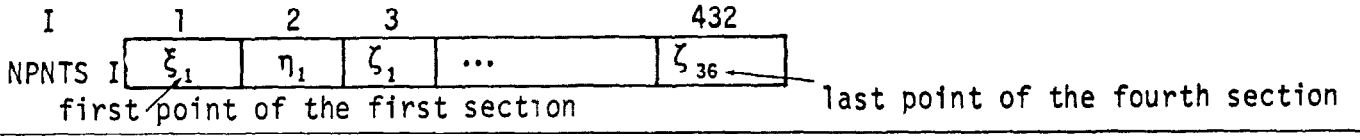

Figure F-9. Numbering Convention and Data Structure

SEARCH. Subroutine HORIZ fills an auxilliary array with the coordinates of 10 points that are on a grid line (η = constant, $-1.0 < \zeta < 1.0$) while VERT stores the corresponding data for grid line (ζ = constant, $-1.0 < \eta < 1.0$). The intersection points are stored in array CPIB in the order they are found. The data is subsequently sorted so that the first data triplet corresponds to the intersection point with the lowest x value. For example, for the intersection case shown in Figure F-10 the initial and final arrangement of data in array CPIS will be as shown.

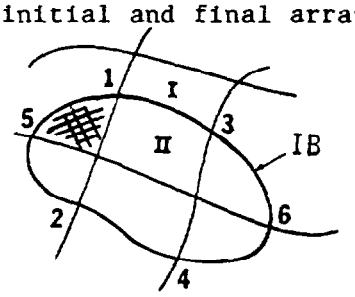

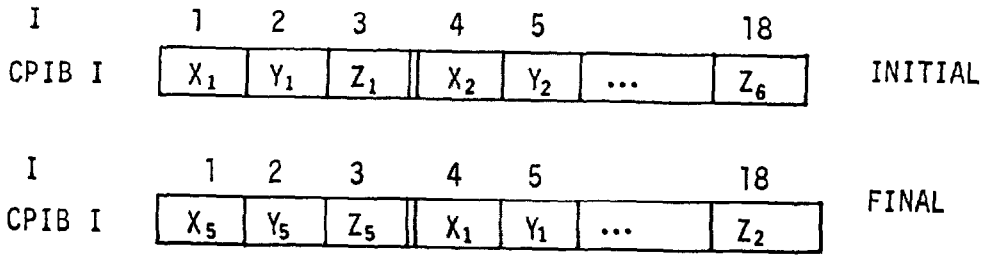

Figure F-10 Determination of the Intersection Points of the Grid Lines with the Inner Boundary

With the data in the CPIB array as shown, the existence of a region with only three edges (such as the hatched region) can be checked. This is done by comparing pairs of adjacent points in CPIB. If the two adjacent points are either on two different vertical or two different horizontal grid lines the region is a regular region. Otherwise, the region is three-sided and another point mid-way between the two points under consideration must be found. This is accomplished by function MID. Array IPNIR contains pointers to the location of the above auxiliary points and all the generated data for inner boundary is stored in array CPNIB.

(16) Subroutine SEARCH. Subroutine SEARCH performs the search to determine whether any pair of points, as shown in Figure F-8, that are on a given grid line are located on a different side of the boundary of IB region, i.e., whether they are both inside, outside, or one inside and the other outside of the inner boundary region. The last situation corresponds to a possible intersection. The point so determined is next checked to assure that the grid line is not tangent to the inner boundary, if the intersection is indeed a true intersection point, the other intersection point on the same grid line is determined next. To check for determination of the point of intersection is done by utilizing the information obtained from the subroutine READ, i.e., the values XMIN, XMAX, YMIN, and YMAX defining the extremum values of the given boundary.

4. Generation of Three-Dimensional Mesh for a Thin Shell Element

There are various ways of generating a mesh of thin shell elements on the surface of the body. For the problem under consideration in the present study the following scheme is proposed on a preliminary basis:

(1) Referring to the procedure outlined previously for plane cross sections, initially a set of twelve control points ($M_{ob} = 12$) is used.

(2) Starting, with the j-th cross section, the first four control points, 7, 8, 9, 10 on the j-th and 1, 2, 3, 4 on the (j + 3) -rd cross sections (See Figure F-11 are chosen as the nodal points on two opposite edges of an isoparametric thin shell element of cubic order.

(3) By selecting the first and fourth control points 6, 11 and 5, 12 of cross sections j + 1 and j + 2, the remaining nodal points necessary for the definition of the other two opposite sides of the element are obtained. This set of 12 nodal points is used in conjunction with the shape functions given below. In this manner, a coarse isoparametric element is generated representing a subregion on the outer surface of the anatomical component under consideration.

(4) Continuing in this manner 3 more isoparametric thin shell elements are generated spanning the group of four cross sections. It should be noted that if successive cross sections are spaced too closely, some of the cross sections are skipped in order to maintain the proper aspect ratios of the elements.

(5) This process is repeated for the next group of four sections, etc., until the entire outer surface of the body is subdivided into subregions.

(6) Based on user specified input, each subregion is criss-crossed by closely spaced grid lines defining isoparametric thin shell elements. This is done through a mapping process using a plane square element in the integer space.

(7) Improvements are preformed, if necessary, on the original mesh by relocating certain node points either by analytical means or interactive graphic processes. Also, in case there are user specified points marking a physical separation curve, joint, etc., care is exercised to locate some of the node points near several of such control points.

The shape functions to be used in the above process are shown below with reference to the numbering scheme shown in Figure F-11.

Point 1: $\xi = -1,\ \eta = +1$

$$N_1 = 1(1 - \xi)(1 + \eta)[9(1 + \eta^2 + \xi^2) - 19]/32 \quad (37)$$

Point 2: $\xi = -1/3,\ \eta = +1$

$$N_2 = 9(1 - \xi^2)(1 - 3\xi)(1 + \eta)/32 \quad (38)$$

Point 3: $\xi = +1/3,\ \eta = +1$

$$N_3 = 9(1 - \xi^2)(1 + 3\xi)(1 + \eta)/32 \quad (39)$$

Point 4: $\xi = +1,\ \eta = +1$

$$N_4 = 1(1 + \xi)(1 + \eta)[9(1 + \eta^2 + \xi^2) - 19]/32 \quad (40)$$

Point 5: $\xi = +1,\ \eta = +1/3$

$$N_5 = 9(1 - \eta^2)(1 + 3\eta)(1 + \xi)/32 \quad (41)$$

Point 6: $\xi = +1,\ \eta = -1/3$

$$N_6 = 9(1 - \eta^2)(1 - 3\eta)(1 + \xi)/32 \quad (42)$$

Point 7: $\xi = +1,\ \eta = -1$

$$N_7 = 1(1 + \xi)(1 - \eta)[9(1 + \eta^2 + \zeta^2) - 19]/32 \quad (43)$$

Point 8: $\xi = +1/3,\ \eta = -1$

$$N_8 = 9(1 - \xi^2)(1 + 3\xi)(1 - \eta)/32 \quad (44)$$

Point 9: $\xi = -1/3,\ \eta = -1$

$$N_9 = 9(1 - \xi^2)(1 - 3\xi)(1 - \eta)/32 \quad (45)$$

Point 10: $\xi = -1,\ \eta = -1$

$$N_{10} = 1(1 - \xi)(1 - \eta)[9(1 + \eta^2 + \xi^2) - 19]/32 \quad (46)$$

Point 11: $\xi = -1,\ \eta = -1/3$

$$N_{11} = 9(1 - \eta^2)(1 - 3\eta)(1 - \xi)/32 \quad (47)$$

Point 12: $\xi = -1,\ \eta = +1/3$

$$N_{12} = 9(1 - \eta^2)(1 + 3\eta)(1 - \xi)/32 \quad (48)$$

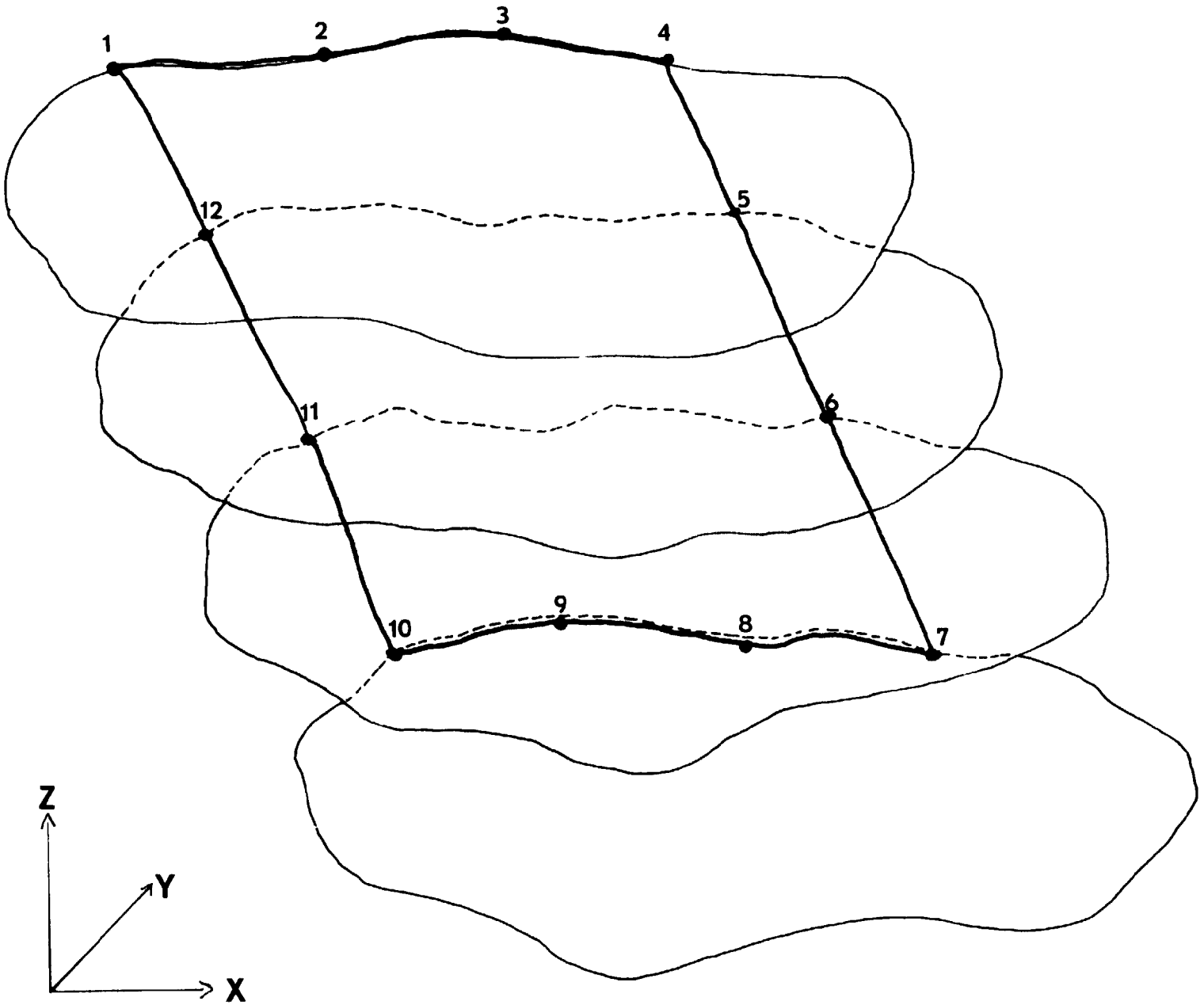

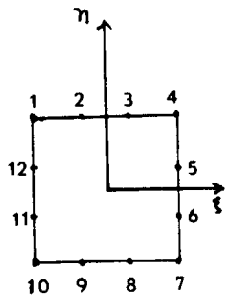

Figure F-11. Thin Shell Element Spanning Four Cross Sections

5. Summary

A computer software package has been developed for generating finite element meshes of selected anatomical components. This has been accomplished by using the data from cross-sectional CT images of the anatomical components under consideration. Some of the basic steps involved in the generation of the finite element mesh are briefly summarized below:

a. For each cross section, arrays containing the coordinates of discrete points on the outer and inner boundaries (if any) of the internal organ are generated and stored in the computer.

b. Considering one cross section at a time, these discrete points are used as the basis of establishing a set of control points on the outer boundary of the cross section.

c. Based on isoparametric element concepts, the control points are used to generate smoothed boundary curves and curvilinear grid lines which subdivide the cross-sectional area into coarse quadrilateral subregions. If some of these subregions do not exhibit the desired shapes and aspect ratios, improvements are performed by means of interactive computer graphics process.

d. Corresponding subregions from successive cross sections are in turn utilized to subdivide the anatomical component into a set of initially coarse three-dimensional isoparametric elements of cubic order.

e. Using isoparametric formulation each of the above elements is associated with a cubical volume in the integer space, and through a mapping process generates a more refined curvilinear mesh for each subregion of the internal body based on user specified input information. This leads to a three-dimensional grid defining the corner nodes of the finite elements corresponding to the level of discretization selected by the user of the program.

f. In case of inner cavity or inner region of different material properties exists, the above procedure is modified to account for the presence of an inner region. For each cross section that intersects the inner cavity, we use a process similar to the generation of the outer boundary to define an inner boundary curve based on the discrete points generated in the scanning process. The intersection points of the grid lines with the inner boundary are then determined. These intersection points, together with previously determined neighboring grid points, are used to split up cross-sectional elements which overlap between the inner and outer regions into distinct quadrilateral elements lying completely within or completely beyond the inner boundary curve. Whenever applicable, this subdivision is maintained in defining the three-dimensional isoparametric elements that span between cross sections.

g. The resulting finite element mesh is displayed graphically, and allowance is made for relocating certain points through an interactive mode, thereby permitting the use to make some final adjustments.

Proposed Extensions -- Extensions of the above work are necessary with the following objectives in mind:

a. To establish a proper link between the mesh generation package developed under the previous project and the finite element analysis package being developed by Dr. Taylor of the University of California.

b. To modify some parts of the mesh generation package in order to achieve greater accuracy in the development of the discrete model representing a given anatomical component.

c. To enhance the mesh generation software package to allow for the modeling of more complex systems involving more than one inner region within an anatomical component. These inner regions may represent inner cavities

or different material properties.

Items a and b may require more elaborate discussion. Relative to the link between the mesh generation and finite element analysis packages, it should be noted that the three-dimensional hexahedral element available in the element library of Dr. Taylor's finite Element Code are the 8, 16, and 20 node brick elements. The 8 node element requires only the specification of corner nodes. Since the mesh generation package automatically establishes the corner nodes for each element, in this case no additional nodal information need be generated. In the case of the 20 node brick element, however, a midside node is needed on each side of the three-dimensional element in order to provide the necessary accuracy in the interpolation process involving such an element. Likewise, midside nodes are needed for the use of any of these three elements, and for the automatic generation of additional nodal points when needed.

A further work on the generation of additional nodes may be necessary here. First of all, the locations of these midside nodes do not coincide with the midside nodes generated for display of the coarse mesh. It is proposed to replace the intermediate nodes (ref. Figure F-7) and the nodes defined as the result of generation of the final mesh with the nodes generated to incorporate the lower degree elements. Secondly, the element node numbering in the current mesh generation program will be modified to correspond to the scheme used in FEAP74 (Dr. Taylor's Finite Element Software Package). Inner regions are sometimes present within the anatomical component. When this configuration occurs, a greater accuracy in the discretization process is needed. Improved accuracy in the discretization processes can be gained for those isoparametric elements lying immediately inside and outside the inner boundary of a cross section by performing interpolation in the normal direction (z-direction) to

establish the possible intersection of the element with the bounding surface of the inner region under consideration. This procedure may lead to further splitting up of elements in a three-dimensional sense in order to distinguish between elements inside or outside the boundary surface.

This result will be accomplished through a curve fitting process using corresponding points between associated cross sections. In this manner, space curves will be generated along the boundary surface of the inner region. These curves with any grid line can then be determined following standard procedures. Such intersections will generate additional nodal points improving the finite element representation.

SECTION G

CONCLUSIONS

Computerized tomographical scanning technique was used to study the anatomical cross-sectional geometers and mass density distribution for children. A total of eight specimens were scanned in the supine position at 1 cm interval and five were selected for the cross-sectional geometry and mass distribution study. Child specimens were very sparse and even when available it was extremely difficult to obtain permission to perform the scanning. Among these specimens one of them was donated to the Department of Anatomy. Permission was granted by the department to scan the body at various positions. Supine, prone and sitting positions were scanned with the specimen under 40°F and frozen conditions. Some anatomical variances both structurally and geometrically due to the scan position were observed. These variances should be taken into consideration for mathematical modelling of human structures.

From each cross-sectional scan of these five selected specimens two types of information were extracted. First, the geometrical data consisted of the boundary coordinates of the cross section and the boundary coordinates of selected anatomical components in that section. Secondly, the mass density distribution of the section included its total mass, geometrical center, center of gravity and inertia tensor. The geometrical data was derived by using standard pattern recognition techniques on the scan picture. The computer program for this procedure had been integrated into the FS0200 scanner computer system which was compatible to the PDP 11/34 computer system. The mass density distribution was obtained by first converting CT numbers to mass densities for all points in each cross section and then appling standard

discrete mass formulas in mechanics to these points.

In order to store this massive information, a data base structure was designed. The implementation of this data base is essential for information retrieval. Due to the special structure of scan picture data format, the scan picture could be retrieved only by using the FS0200 scanner computer system. With the implementation of the data base, the scan pictures as well as the extracted information would have a uniform data format and hence it would be transferable to any computer system.

A discretization procedure and the generation of an internal mesh from boundary coordinates of an anatomical component to be used for finite elements analysis was also presented. Given the three-dimensional coordinates of an anatomical component extracted from scan pictures, this mesh generator generated an internal mesh for this structure ready to be used by the finite elements analysis.

The methodology presented in this report was the only nondestructive technique available at the present time for obtaining cross-sectional geometry and mass density distribution of the human body. The data presented in this volume and Volume II on the five children specimens is original in both its nature and the method of derivation. Similar methodology can be applied to study injury criteria due to impact. This can be accomplished by comparing the difference between pre-impact and post-impact CT scans using animal models. Some other immediate applications of this data are inputs to finite elements, and lumped parameter biodynamic models, computer simulation of vehicle crash victims (16,17) and designing carsh dummies.

SECTION H

FUTURE STUDIES

The following topics are recommended for future studies.

1. Development of geometric correction rules to modify a base internal (visceral) and external (body contours) geometry from the specimens so that newly derived geometry can be obtained.

The geometry correction rules were supposed to be derived from three sources (with emphasis on the scanning subject):

(1) Scanning Subjects: by incorporating the height, weight, age and sex of five scanning subjects as parameters.

(2) Autopsy Report from the Children's Hospitals: by incorporating the autopsy reports on the sizes of various organs as a function of age, height, weight and sex.

(3) Various Handbooks: by incorporating tables of weights of various organs in infancy and in childhood from pediatric handbooks (18) and autopsy handbooks.

However, experience from these few years told us that child geometry, especially internal organ geometry, varied a great deal, even within the same age group. The five specimens in the study population were not sufficient to serve as primary souces in developing the geometric correction rule. Employing autopsy reports and data from handbooks is also inadequate for data interpretation, because the majority of these data used weight vs. age and sex as the sole measuring parameter. There are two remedial approaches: Utilize a large sample of measurements from autopsy results. To this end it is possible to collaborate with the Pathology Department of Children's Hospital to get access into the data file. This collaboration will entail the transmission of autopsy reports and the involvement in measuring the pertinent parameters

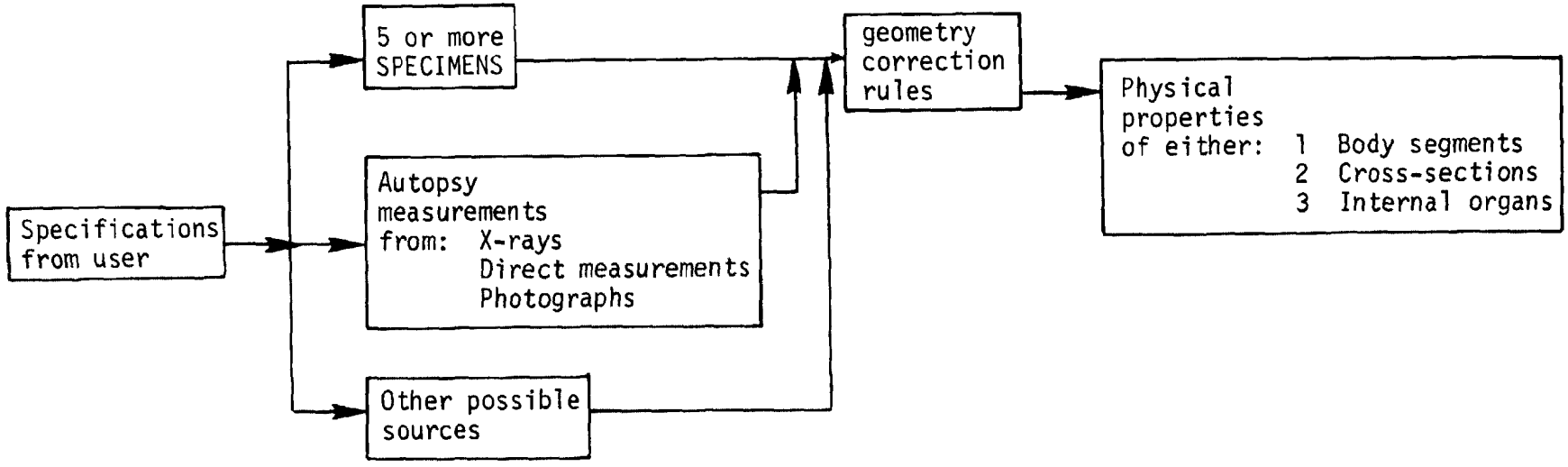

Figure Block Diagram Showing the Derivation of Geometry Correction Rules.

Figure H-1. Block Diagram showing the derivation of geometry correction rules.

which would include the weight and shape of internal organs. After incorporating these measurements with the data from the five specimens already scanned, the geometric rules derived should be more reliable.

A second possible approach entails the scanning of more specimens, a strategy which would seem to suffer from the sparse number of specimens in the age group required.

The diagram on the preceeding page shows the proposed procedure for carrying out this phase of the research.

2. Extension and Modification of the Computer Software for the Generation of the Finite Elements Mesh

2.1 Previous Work

A computer software package had been developed under the present study for generating finite elements meshes of selected anatomical components. This had been accomplished by using the data from cross-sectional CT images of the anatomical components under consideration. Some of the basic steps involved in the generation of this finite element mesh are outlind below: (See Section F for further detailed explanations.)

(1) For each cross section arrays containing the coordinates of discrete points on the outer and inner boundaries (if any) of the internal organ are generated and stored in the computer.

(2) With one cross section considered at a time, these discrete points are used as the basis of establishing a set of control points on the outer boundary of the cross section.

(3) Based on isoparametric element concepts, the control points are used to generate smoothed boundary curves and curvilinear grid lines which subdivide the cross-sectional area into coarse quadralateral subregions. If some of these subregions do not exhibit the desired shapes and aspect ratios, improvements are performed by means of an interactive computer graphics process.

(4) Corresponding subregions from successive cross sections are in turn utilized to subdivide the anatomical component into a set of initially coarse three-dimensional isoparametric elements of cubic order.

(5) Using isoparametric formulation each of the above elements is associated with a cubical volume in the integer space, and through a mapping process generates a more refined curvilinear mesh for each subregion of the internal body based on user specified input information. This leads to a three-dimensional grid defining the corner nodes of the finite elements corresponding to the level of discretization selected by the user of the program.

(6) In case an inner cavity of an inner region of different material properties exists, the above procedure is modified to account for the presence of an inner region. For each cross section that intersects the inner cavity a process similar to the generation of the outer boundary is used to define an inner boundary curve based on the discrete points generated in the scanning process. The intersection points of the grid lines with the inner boundary are then determined. These intersection points are used to split up cross-sectional elements which overlap between the inner and outer regions into distinct quadrilateral elements completely within or completely beyond the inner boundary curve. Whenever applicable, this subdivision is maintained in defining the three-dimensional isoparametric elements that span between cross sections.

(7) The resulting finite element mesh is displayed graphically, and allowance is made for relocating certain points through in interactive mode, thereby permitting the user to make some final adjustments.

2.2 Extensions of the Present Work

The following extensions of the present work is recommended.

(1) To establish a proper link between the mesh generation package developed under the previous project and the finite element analysis package being developed by Dr. Taylor of the University of California.

(2) To modify some parts of the mesh generation package in order to achieve greater accuracy in the development of the discrete model representing a given anatomical component.

(3) To enhance the mesh generation software package to allow for the modelling of more complex systems involving more than one inner region within an anatomical component. These inner regions may represent inner cavities or regions of different material properties.

3. Scan Five Adult Specimens of Various Sizes and Create an Adult Data Base for Various Simulation Studies

3.1 Description

An adult specimens data base should be established. This can be accomplished by first scanning five adult specimens of various sizes and then extracting relevant data from scanning pictures. This complete human subject data base can be used in many different kinds of studies, among which are comptuer simulations, design of dummies, modeling. In order to obtain this data base, the following steps is recommended:

1) Select five adult specimens of various sizes.

2) Scan these five specimens.

3) Extract boundaries of:

   a) Cross sections
   b) Anatomical structures described in this report.

4) Store all inforamtion in the data base described in Section (D).

4. Derivation of Various Configurations of Body Geometry and Mass Density Distribution

It is important to know various configurations of body geometry and distributions before the impact condition. These parameters can be obtained by the following approach.

1) Specimen Preparation - a three dimensional grid pattern will be created inside a specimen so that in a cross-sectional scan a two dimensional grid pattern will be visible in the scan picture.

2) Scanning Positions - The prepared specimen will be frozen in several positions before scanning. These scanning positions will serve as a basis for interpolating body geometry and density distribution for various possible configurations.

3) Interpolating Body Geometry and Density Distribution.

4.1 Specimen Preparation

Two alternative methods of specimen preparation should be investigated. Both methods use rubber silicon (or other radiopaque material) and similar experimental apparatus.

1) Method I

a. Rubber Silicon (RS, Radiopaque) will be injected into flexible polyethylene tubes of a certain diameter size (to be determined) either continuously or in a dot pattern of prescribed distances between dots. The injection will be done by a fine, long needle. The rubber silicon will solidify inside tubes within about five minutes after the injection.

b. A transparent platform table will be used for supporting the

specimen. A frame structure with specific marks (or coordinate points) and guiding rods will be placed on the top of the table. This frame will serve as the reference for inserting polyethylene tubes into the specimen. (See Figure H-2.)

c. A properly prepared specimen will be placed on top of the platform table and beneath the frame structure. Polyethylene tubes will be inserted into the specimen longitudinally through guiding rods. As a result a three-dimensional cross pattern of polyethylene tubes will be formed inside the body. (See Figure H-3.)

2) Method II

The advantage of the first method is that polyethlene tubes are relatively easy to insert into the body. The disadvantage is the possibility of reducing the shift mobility of body organs and tissues due to the addition of tubings which might act as anchors. Another approach is the direct injection of rubber silicon into a specimen by using the guiding rods of the frame. The rubber silicon can be injected through a needle into the specimen at various depths by the addition of a depth-guide attached to the guiding rods assembly. This method will produce a three-dimensional radiopaque dot pattern inside the specimen. The augmentation of this foreign dot pattern inside the body will not reduce the shift mobility of body organs and tissues as much as that of the polyethylene tubing. The advantage of this method is the silicon rubber may get lost in cavities such as the stomach, lumen of blood vessels, gastrointestinal tracts, heart chambers, trachea, bronchii, inter-tissue, inter-organ spaces, thoracic cavity, and abdominal cavity. One possible remedy is to avoid injecting the rubber silicon into these cavities. For this purpose, a bi-plane flouroscopic technique may be used to guide the injection procedure.

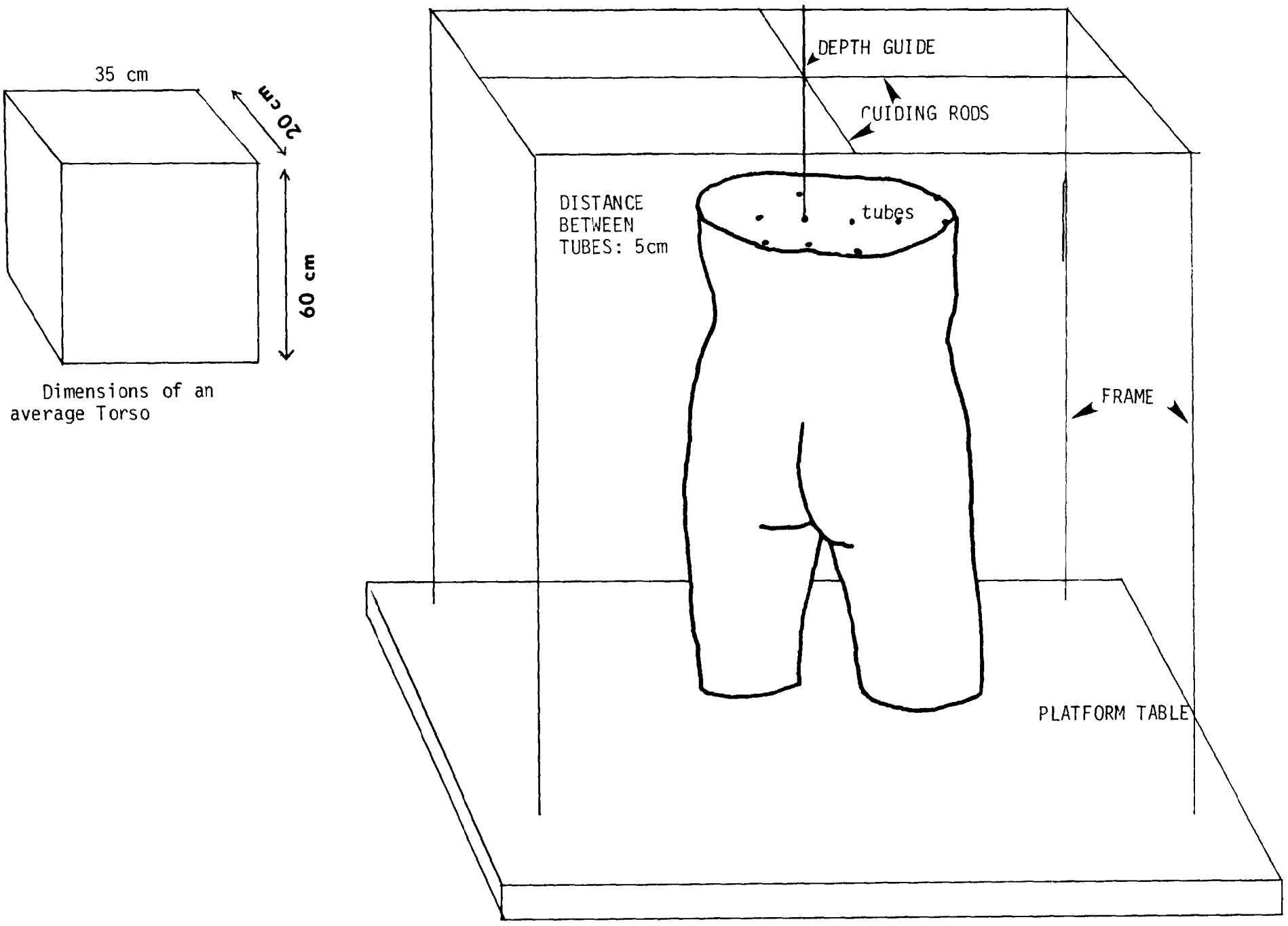

Figure H-2. Experimental Set-up for Injecting Radiopaque Material into a Specimen.

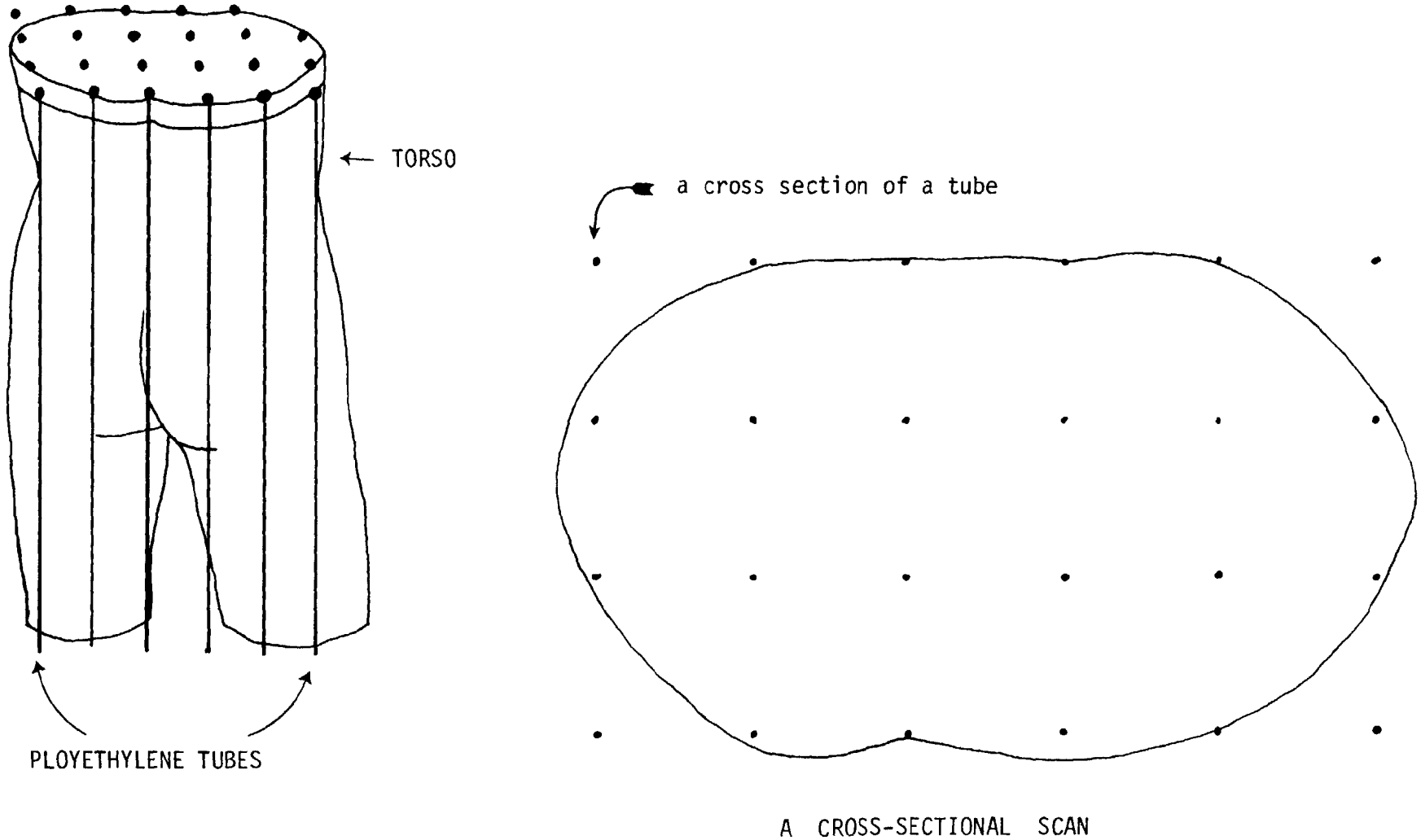

FIGURE H.3Three-Dimensional Tubing and a corresponding cross section.

a. Scanning Positions

The specimen will be frozen in the following positions desribed by the spherical coordinate system. (See Figure H-4.)

(1) Standing: (or sitting) $\theta = 0$, $\phi = 0°$

(2) Semi-prone: $\theta = 0$, $\phi = 45°$.

(3) Right lateral: $\theta = -90°$, $\phi = +45°$

(4) Left lateral: $\theta = 90°$, $\phi = +45°$.

(5) Semi-prone, right oblique: $\theta = -45°$, $\phi = +45°$.

(6) Semi-prone, left oblique:* $\theta = +45°$, $\phi = 45°$.

The specimen will be frozen with the temperature of -10°F in one of these positions in the freezer for two days. The frozen specimen will be scanned perpendicular to the body axis. After the scan, the body will be thawed for two days at room temperature. The body will then be frozen in a second position and so on until all positions have been scanned.

b. Interpolating Body Geometry and Density Distribution

Once CT scans of these positions are obtained, the body geometry and density distribution can be extracted by using methods described in this report. Other positions can also be derived by using interpolation.

*This terminology is after Dr. F. Suarez, M.D., Department of Anatomy, Georgetown University Medical School.

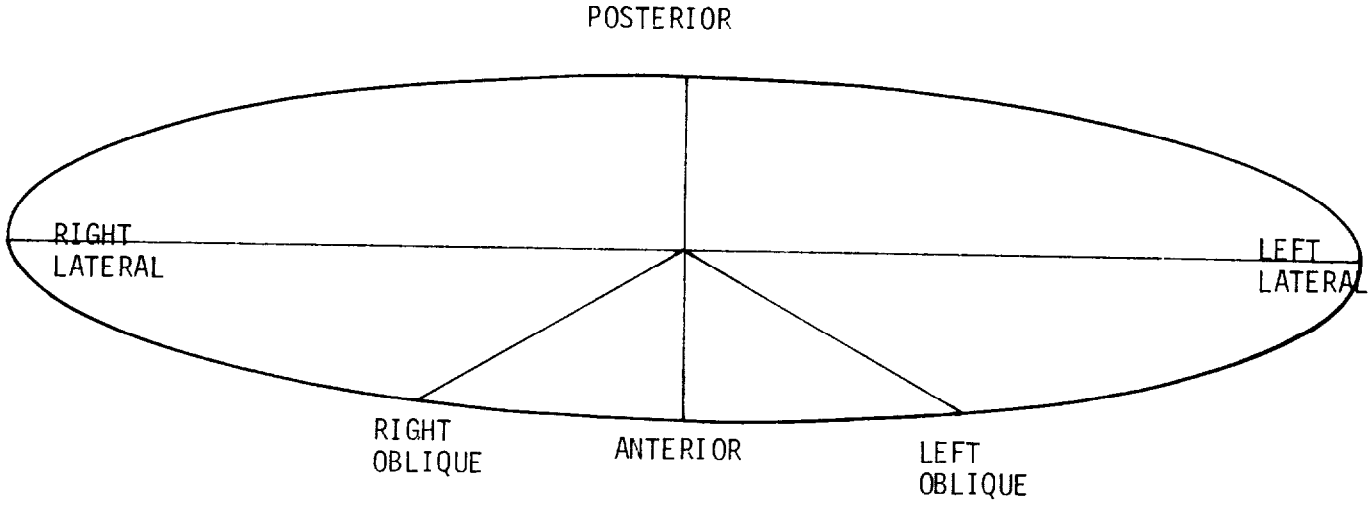

(a)

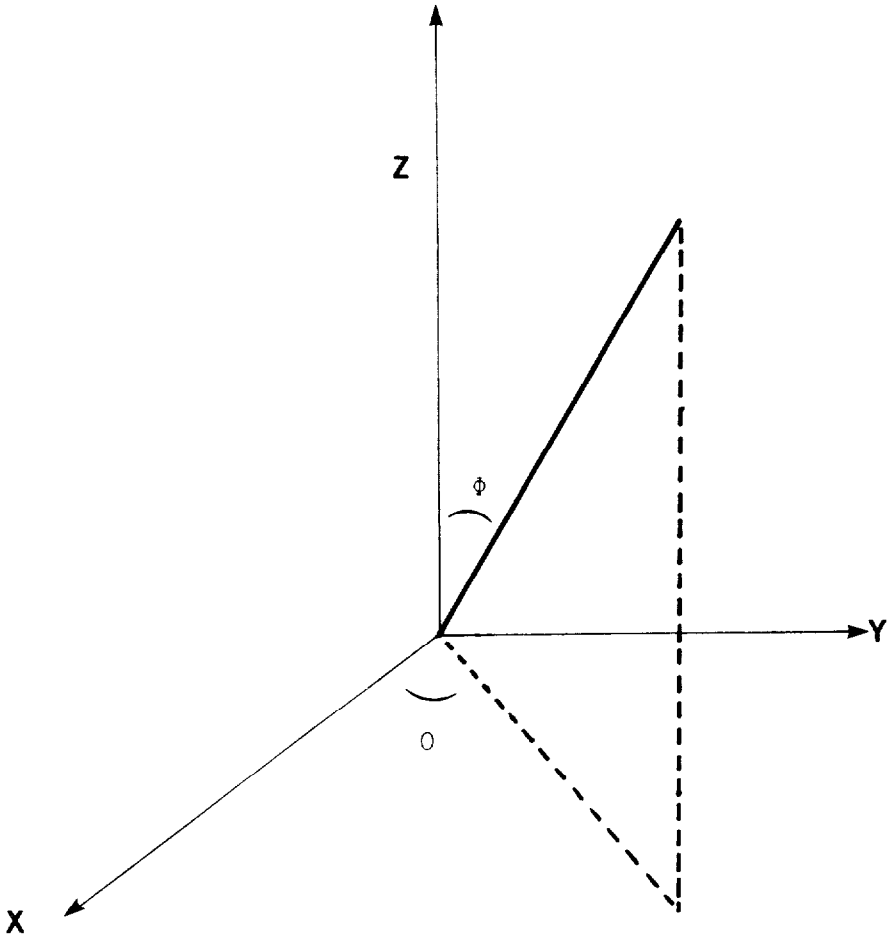

(b)

Figure H.4 (a) Terminology used for frozen positions
(b) Spherical Coordinate System

SECTION I

REFERENCES

1. Y.K. Liu and J.K. Wickstrom, "Estimation of the Inertial Property Distribution of the Human Torso from Segmented Cadaveric Data," Perspectives in Biomedical Engineering. pp. 203-213, 1973.

2. W.S. Snyder, Report of the Task Group on Reference Man, Pergamon Press, 1975.

3. D.U. Goulet, J.R. Cuzzi, R.E. Heron, "A Parametric Description of the Human Body Using Biosterometric Techniques," Am. Soc. Photgrammetry, Falls Church, VA, 1974.

4. J. Ambrose, et al., "Computerized X-Ray Scanning of the Brain," J. Neurosurg., 40:679-695, 1974.

5. R.S. Ledley, et al., "Computerized Transaxial X-Ray Tomography of the Human Body," Science, 186:207-212, Oct. 1974.

6. H.K. Huang, S.C. Wu, "The Evaluation of Mass Densities of the Human Body in vivo," Comp. Biol. Med. 6(4):337-343, Oct. 1976.

7. ACTA Model FS0200 Scnner, Operating Instructions, Pfizer Medical Systems, Inc., May 1977.

8. H.K. Huang, Men Fai Shiu, O. Steiner, R.S. Ledley, "Selected Computerized Tomographic Scan Data Format," Proc. Computer Society Conference on Pattern Recognition and Image Processing (IEEE), pp. 438-443, June 1978.

9. M. Green, J.B. Richmond, Pediatric Diagnosis, 2nd ed., W.B. Saunders, 1968.

10. J.C. Mazziotta, H.K. Huang, "THREAD (Three-Dimensional Reconstruction and Display) with Biomedical Appliations in Neuron Ultrastructure and Computerized Tomography," AFIPS Conference Proceedings, 45:250-251.

11. H.K. Huang, J.C. Mazziotta, M.J. Cerroni, "Computer Processing or Computerized Tomography Scans," Proceedings of the First Annual Symposium of Computer Applications in Medical Care, Washington, DC, pp. 356-362, Oct. 1977.

12. H.K. Huang, "Fundamentals of Biomedical Image Processing," Proceedings of the Second Annual Symposium of Computer Applications in Medical Care, Washington, DC, pp. 8-14, Nov. 1978.

13. Desai, C.S and Abel, J.F., "Introduction to the Finite Element Method," van Nostrand Reinhold Company, New York, 1972.

14. Gallagher, R.H., "Finite Element Analysis Fundamentals," Prentice Hall, Inc., Englewood Cliffs, NJ, 1975

15. Computer Graphics, A Quarterly report of Siggraph-ACM. Vol. II, No. 3, Fall, 1977.

16. J.T. Fleck, F.E. Butler, and S.L. Vogel, "An Improved Three-Dimensional Computer Simulation of Vehicle Crash Victims," Volume Nos. 1 through 4, Report Nos. DOT-HS-801-507, 508, 509, and 510, April 1975. (Final Report for Contract No. DOT-HS-053-2-485).

17. M.M. Reddi, et al., "Thoracic Impact Injury Mechanism," Volumes 1 and 2, Report Nos. DOT-HS-801-710 and DOT-HS-801-711, August 1975. (Final Report for Contract No. DOT-HS-243-3-424).

18. W.E. Nelson, V.C. Vaughan, R.J. McKay, Testbook of Pediatrics, 9th ed., chapter 2, W.B. Saunders, 1969.